3. ATMOSPHERIC MEASURMENTS

Jürgen Graeser[1], Anja Sommerfeld[1], Tercio Silva[3], Wessley King[4], Steele Griffiths[3], Hannes Griesche[8], Taneil Uttal[6], Michael Gallagher[5,6], Dean Howard[15,6]. Ivo Beck[21],

(not on board) Markus Rex[1,2], Marion Maturilli[1], Alexander Schulz[1], Matthew Shupe[5,6], Heath Powers[3,4], Jim Mather[3,7], David Chu[3,4], Ronny Engelmann[8], Martin Radenz[8], Julian Hofer[8], Dietrich[8], Holger Baars[8], Patric Seifert[8], Albert Ansmann[8], Andreas Macke[8], Mario Mech[9], Bernhard Pospichal[9], Kerstin Ebell[9], Susanne Crewell[9], Gaël Dubois[10], Luc Blarel[10], Philippe Goloub[10], Ola Persson[5,6], David Costa[5,6], Ian Brooks[11], Thomas Ayers[6], Christopher Cox[6], Christopher Fairall[6], Daniel Gottas[6],Jesse Leach[6], Sara Morris[6], Jackson Osborn[5,6], Sergio Pezoa[6], Jennifer Hutchings[12], Don Perovich[13], Timothy Stanton[14], Roberta Pirazzini[15], Byron Blomquist[5,6], Detlev Helmig[5], Steve Archer[16], Laurens Ganzeveld[17], Jacques Hueber[5], Christopher Fairall[6], Dean Howard[5], Ludovich Bariteau[5,6], Kevin Posman[16], Hans-Werner Jacobi[18], Helene Angot[5], Sjoerd Barten[17], William Sturges[19], Lucy Carpenter[20], Lauriane Quéléver[22], Julia Schmale[21], Mikko Sipilä[22], Tiia Laurila[22], Tuija Jokinen[22], Zoe Brasseur[22]

[1]DE.AWI
[2]DE.UNI-Potsdam
[3]GOV.ARM
[4]GOV.LANL
[5]EDU.CU
[6]GOV.NOAA
[7]GOV.SANDIA
[8]DE.TROPOS
[9]DE.UNI-KOELN
[10]FR.UNIV-LILLE
[11]UK.UNI-LEEDS
[12]EDU.ORSU
[13]EDU.DARTMOUTH
[14]EDU.NPS
[15]FI.FMI
[16]ORG.BIGELOW
[17]NL.WUR
[18]FR.UGA
[19]UK.AC.UEA
[20]UK.AC.YORK
[21]CH.EPFL
[22]FI.UNI-Helsinki

Grant-No. AWI_PS122_00

A comprehensive summary of the atmospheric measurements during all 5 cruise legs can be found in Shupe et al., 2022.

References

Shupe, MD, Rex, M, Blomquist, B, Persson, POG, Schmale, J, Uttal, T, Althausen, D, Angot, H, Archer, S, Bariteau, L, Beck, I, Bilberry, J, Bucci, S, Buck, C, Boyer, M, Brasseur, Z, Brooks, IM, Calmer, R, Cassano, J, Castro, V, Chu, D, Costa, D, Cox, CJ, Creamean, J, Crewell, S, Dahlke, S, Damm, E, de Boer, G, Deckelmann, H, Dethloff, K, Dütsch, M, Ebell, K, Ehrlich, A, Ellis, J, Engelmann, R, Fong, AA, Frey, MM, Gallagher, MR, Ganzeveld, L, Gradinger, R, Graeser, J, Greenamyer, V, Griesche, H, Griffiths, S, Hamilton, J, Heinemann, G, Helmig, D, Herber, A, Heuzé, C, Hofer, J, Houchens, T, Howard, D, Inoue, J, Jacobi, H-W, Jaiser, R, Jokinen, T, Jourdan, O, Jozef, G, King, W, Kirchgaessner, A, Klingebiel, M, Krassovski, M, Krumpen, T, Lampert, A, Landing, W, Laurila, T, Lawrence, D, Lonardi, M, Loose, B, Lüpkes, C, Maahn, M, Macke, A, Maslowski, W, Marsay, C, Maturilli, M, Mech, M, Morris, S, Moser, M, Nicolaus, M, Ortega, P, Osborn, J, Pätzold, F, Perovich, DK, Petäjä, T, Pilz, C, Pirazzini, R, Posman, K, Powers, H, Pratt, KA, Preußer, A, Quéléver, L, Radenz, M, Rabe, B, Rinke, A, Sachs, T, Schulz, A, Siebert, H, Silva, T, Solomon, A, Sommerfeld, A, Spreen, G, Stephens, M, Stohl, A, Svensson, G, Uin, J, Viegas, J, Voigt, C, von der Gathen, P, Wehner, B, Welker, JM, Wendisch, M, Werner, M, Xie, ZQ, Yue, F. 2022. Overview of the MOSAiC expedition: Atmosphere. Elementa: Science of the Anthropocene 10(1). DOI: https://doi.org/10.1525/elementa.2021.00060

3.1 FROM THE SURFACE TO THE STRATOSPHERE: CHARACTERIZATION OF THE ATMOSPHERIC COLUMN

Jürgen Graeser[1], Anja Sommerfeld[1] [1]AWI
(not on board:) Markus Rex[1,2], Marion Maturilli[1], Alexander Schulz[1] [2]DE.UNI-Potsdam

Objectives

To investigate the thermodynamic, turbulence and trace gas parameters at the ice-atmosphere interface, in the planetary boundary layer (PBL), in the free atmosphere and the lower stratosphere, several platforms like a mobile eddy covariance system and 10 m mast, a tethered and weather balloons are used.

a) Turbulent energy fluxes over sea ice and over leads

The turbulent exchange within the PBL of the atmosphere is not well understood, therefore models show a wide spread in predicting turbulent fluxes due to strong overestimation and underestimation of its magnitude. The reasons are insufficient parameterizations of the turbulent exchanges that result from a very limited amount of datasets measured during short campaigns. The SHEBA campaign (Uttal et al., 2002) that also measured over a full annual cycle in the Beaufort Sea was over 22 years ago in markedly different time and region. Especially the studies of the turbulent exchange over open leads on sea ice in the high Arctic are very rare due to a very small number of campaigns like ALEX within AIDJEX (Andreas et al., 1979), LEADEX (Ruffieux et al., 1995) and STABLE (Tetzlaff et al., 2015). However, these datasets do not cover the full spectrum of atmospheric conditions, seasons or surface characteristics. Hence, the parameterizations do not include all relevant processes or only in an insufficient way.

Due to the concept of MOSAiC, allowing observations for an entire year, it is possible to measure the turbulent exchange during a full annual cycle. We use the newest generation of *in-situ* turbulence sensors to observe nearly all relevant surface characteristics. For that purpose, mobile eddy covariance towers will be installed at the edge of open leads and close to ridges on the sea ice, in such a way that the targeted areas are directly within the footprint of the instrument. In addition, a net radiometer will measure all four radiation components over the open water during observing at open leads, contributing to the complete surface energy balance. Furthermore, pronounced changes in the surface characteristics like a change of thermal conditions (open leads, warm water) or ridges (high obstacles, strong friction) result in the development of internal boundary layers on the lee side of the targeted area. Especially for thermal internal boundary layers (over open leads) both, the height and the temporal evolution were very seldom observed so far, resulting in a small number of data points and a wide spread (see e.g. Andreas et al., 1999). Therefore, a 10 m mast with an optical fibre cable (Distributed Temperature Sensor, DTS system) measuring the air temperature every 60 cm (25 cm sampling length) and 5-10 s will be installed next to the mobile eddy covariance system for observing the temporal evolution of the thermal internal boundary layer.

b) Characterization of the planetary boundary layer over sea ice

The PBL is the lowermost atmospheric layer, connecting the surface and the free atmosphere. In the Arctic, and especially during polar night and under high pressure influence, the Arctic PBL is typically a stable and persistent feature. In the case of stable conditions, exchange with the surface is strongly inhibited, and marked temperature inversions of the order of several Kelvin are common features. In case of neutral conditions, both synoptic and radiative forcing can quickly change turbulence characteristics. The turbulent fluxes of momentum, energy and chemical compounds, as well as surface-based temperature inversions in the Arctic PBL are known to be crucial players in Arctic Warming and sea ice retreat, but are generally poorly resolved in state of the art climate models (Boé et al., 2009, Pavelsky et al., 2012, Holtslag et al. 2013,). This is in parts due to insufficient parameterizations of sub-grid scale processes (Pithan et al., 2014) that have been developed on the basis of only a few dedicated campaigns, such as, for instance, AIDJEX (Andreas et al., 1979), LEADEX (Ruffieux et al., 1995), SHEBA (Uttal et al., 2002) or STABLE (Tetzlaff et al., 2015). Other than during these campaigns, the extraordinary opportunity during MOSAiC is to measure characteristics of the Arctic PBL over sea ice during the course of a whole year, including a variety of different surface characteristics. Monitoring the thermal structure of the PBL is enabled by a state of the art *in-situ* sensor for capturing high frequency temperature fluctuations along a fibre cable (DTS), with 25 cm physical resolution and 10 seconds sampling interval. Using a tethered balloon (TB) as a carrier platform for the DTS, vertical time series of the thermodynamic structure of the PBL will be retrieved, and the potential impact of nearby open leads (open water), ridges (high obstacles) or changing large-scale synoptic forcing will be investigated. This is the first time ever the DTS technology is combined with a TB for such investigations over the central Arctic sea ice.

A suite of additional sensors from other partners and institutes will be occasionally deployed with the TB throughout the course of the year, giving additional insights into the dynamical, thermodynamical and chemical characteristics of the PBL onsite the TB launch platform. These include, e.g. an optical particle sonde, an aerosol particle filter package, an ozone profiler, and a turbulence sensor package. The combined measurements assure the close link to other projects and foster the joint analysis of other atmospheric topics.

c) Characterization of the free troposphere and lower stratosphere

An extensive balloon program will operate from board Polarstern, reaching from upgraded weather balloons to sophisticated research sondes. The profiles obtained by radiosondes launched four times daily will directly support the on-site weather forecast during the expedition, while they further contribute to numerical weather forecast as observational input for data assimilation. Additional Arctic radiosondes are known to positively impact the performance of forecast systems (Yamazaki et al., 2015; Inoue et al., 2015) even in regions far from the Arctic (Sato et al., 2016; 2018). The atmospheric thermodynamic structure over sea ice was recorded by radiosondes during earlier campaigns like e.g. SHEBA (Uttal et al., 2002) or N-ICE2015 (Kayser et al., 2017) for other regions of the Arctic. Now, the atmospheric structure, moisture content, stability, Atmospheric boundary layer (ABL) height, tropopause height and other features in the vertically resolved atmospheric column will be monitored in the Central Arctic for a complete annual cycle. Events of heat and moisture transport into the Arctic by intrusions or atmospheric rivers (Woods and Caballero, 2016; Nash et al., 2018) will be identified, and their impact on the local atmospheric structure analyzed. The combination with projects that focus on the observation of clouds and radiation will allow to focus on the transitions between radiatively clear and cloudy states (Stramler et al., 2011; Graham et al., 2017) and how these transitions impact the vertical stability and coupling within the atmospheric column. The radiosonde profiles retrieved during MOSAiC will be set into context with similar measurements at pan-Arctic land based stations (e.g. Ny-Alesund,

Utqiagvik/Barrow, and other IASOA stations) for studies of the advective connection between the inner and outer Arctic, and the role of the Arctic dome in these exchange processes.

Weekly ozone sonde profiles will characterize the ozone distribution in the tropo- and the stratosphere throughout the year. In winter and spring, they will be part of a potential pan-Arctic ozone sonde campaign (Match) with coordinated soundings at all Arctic ozone sonde stations (e.g. von der Gathen et al., 1995; Rex et al., 1997, 2004; Manney et al., 2011). The aim is to determine the ozone loss inside the polar vortex. We expect new Arctic record ozone losses due to record low temperature regimes in single winters within the future 10 to 20 years (e.g. Rex et al., 2006).

Water vapor is a chemically, physically, and radiatively active trace gas, and its distribution in the stratosphere determines significant climatic implications. The water vapor distribution in the Arctic stratosphere bares evidence for dynamical aspects on different scales, including the large scale descending motion inside the polar vortex as well as filamentary structures at the vortex edge linked to Rossby wave activity (Maturilli et al., 2006). In the presence of very low temperatures, the sedimentation of polar stratospheric cloud (PSC) ice particles can lead to dehydration events (Maturilli and Dörnbrack, 2006; Khaykin et al., 2013). With our monthly balloon-borne cryogenic frostpoint hygrometer (CFH) measurements during MOSAiC we contribute to the assessment of the water vapour distribution in the Arctic stratosphere. The dual soundings with the Compact Optical Backscatter and AerosoL Detector (COBALD) during polar night will allow to identify PSC layers related to dehydration.

Work at sea

a) Onboard Polarstern

Throughout Leg 2 (period from December 13, 09UTC until February 24, 09UTC), 292 weather balloons have been started from the Helicopter deck onboard *Polarstern* in a 6-hourly rhythm. The launch times were chosen after the synoptical hours, i.e. 05UTC, 11UTC, 17UTC and 23UTC.

Weather balloons usually reach a height up to 30 km. However, due to the strong decreasing temperature in the lower stratosphere, the balloons blast too early and reach a height below 20 km. Therefore, before each launch, the balloons were bathed in a mixture of oil and diesel. This bath softens the material, makes it more flexible, and therefore allows the balloon to reach the 30 km height even with the temperatures below -90°C in the lower stratosphere.

In addition to these standard meteorological radiosondes, joint launches with ozone sensors were conducted roughly on a weekly basis. Later during Leg 2, the ozone sondes were launched more often due to the Match campaign. Match is a campaign that is taking place every year during spring to investigate the ozone loss in the polar vortex. With this purpose coordinated launches of ozone sondes in all Arctic launch stations are possible, to probe the same air parcel. A list of all ozone soundings during leg 2 is given in Table 3.1.1, those that were performed in addition to the weekly schedule, because of MATCH, are indicated.

The sounding PS122/2_16-20, PS122/2_20-22, PS122/2_22-40 furthermore incorporates a launch of the CFH and COBALD.

***Tab. 3.1.1**. List of all ozone soundings during leg 2, with device operation (left) and date (right).*

PS122/2_16-20	18.12.2019 17UTC
PS122/2_17-38	25.12.2019 17UTC
PS122/2_18-31	01.01.2020 17UTC
PS122/2_19-50	08.01.2020 17UTC

PS122/2_20-22	14.01.2020 17UTC
PS122/2_21-60	22.01.2020 17UTC
PS122/2_22-40	29.01.2020 11UTC
PS122/2_22-60	30.01.2020 17UTC
PS122/2_23-44	05.02.2020 17UTC
PS122/2_23-104	08.02.2020 17UTC (MATCH)
PS122/2_24-40	12.02.2020 17UTC (MATCH)
PS122/2_25-40	18.02.2020 11UTC
PS122/2_25-70	20.02.2020 17UTC (MATCH)
PS122/2_25-85	21.02.2020 17UTC (MATCH)

b) Onboard Polarstern

- Tethered Balloon platform

For the operation of the tethered balloon (TB), a dedicated launch site, called Balloon Town (BT), has been installed in the Central Observatory during Leg 1. It is close to Ocean City, at approximately 400 m distance to *Polarstern.* For further information about the structure and the set-up of BT, please see the cruise report of Leg 1 and Figure 3.1.1.

The TB has a size of 9 m^3 and is filled with helium. By using a winch, the TB can reach a height up to 1500 m and it can carry a payload of 4-5 kg.

There are two ways to carry out measurements with the TB. First, for continuous measurements, by bringing the TB up to a certain height and leave it there for several hours and second, the profile mode by ascending and descending the TB. The continuous measurement mode was used for the DTS glass fibre temperature profiles and for the aerosol filter sampler from the British Antarctic Survey (BAS). Due to technical problems with the DTS glass fibre, the high frequency temperature measurement could only be performed during the beginning of Leg 2. The aerosol filter sampler was not ready in the beginning of Leg 2 and therefore it was operated only during the end of Leg 2.

For the turbulence sensor from TROPOS, the optical particle counter from BAS and for the ozone sonde from NOAA, it was most sufficient to run the TB in the profile mode. While the turbulence sensor was operated during each flight of the TB, the optical particle counter and the ozone sonde where operated only since January 2020.

During leg 2, 13 days were suitable, concerning the weather conditions with wind speeds below 6 m/s, to launch the tethered balloon, resulting in a total number of 23 launches.

A list of all TB launches and deployed sensors is given in Table 3.1.2.

Fig. 3.1.1: Balloon Town

***Tab. 3.1.2**: List of all TB operations during leg 2.*

Device operation	Sensor	Start time UTC	End time UTC
PS122/2_16-71	Tethersonde	20.12.2019 07:49	20.12.2019 13:46
	DTS	20.12.2019 07:49	20.12.2019 13:46
PS122/2_16-72	Tethersonde	21.12.2019 07:43	21.12.2019 09:57
	Turbulence	21.12.2019 07:43	21.12.2019 09:57
PS122/2_17-13	Tethersonde	23.12.2019 11:10	23.12.2019 11:43
	Turbulence	23.12.2019 11:10	23.12.2019 11:43
PS122/2_17-14	Tethersonde	23.12.2019 11:49	23.12.2019 12:47
	Turbulence	23.12.2019 11:49	23.12.2019 12:47
	DTS	23.12.2019 11:59	23.12.2019 12:41
PS122/2_17-15	Tethersonde	23.12.2019 12:54	23.12.2019 13:25
	Turbulence	23.12.2019 06:05	23.12.2019 06:24
PS122/2_17-96	Tethersonde	28.12.2019 11:35	28.12.2019 13:32
	Turbulence	28.12.2019 11:35	28.12.2019 13:32
	DTS	28.12.2019 12:58	28.12.2019 13:11
PS122/2_17-106	Tethersonde	29.12.2019 07:50	29.12.2019 08:16

	Turbulence	29.12.2019 07:50	29.12.2019 08:16
PS122/2_17-107	Tethersonde	29.12.2019 11:28	29.12.2019 12:10
	Turbulence	29.12.2019 11:28	29.12.2019 12:10
PS122/2_18-98	Tethersonde	05.01.2020 11:51	05.01.2020 12:30
	Turbulence	05.01.2020 11:51	05.01.2020 12:30
PS122/2_18-99	Tethersonde	05.01.2020 13:01	05.01.2020 13:31
	Turbulence	05.01.2020 13:01	05.01.2020 13:32
PS122/2_19-13	Tethersonde	06.01.2020 08:00	06.01.2020 09:23
	Turbulence	06.01.2020 08:00	06.01.2020 09:23
PS122/2_19-14	Tethersonde	06.01.2020 10:57	06.01.2020 11:41
	Turbulence	06.01.2020 10:57	06.01.2020 11:41
PS122/2_19-26	Tethersonde	07.01.2020 07:19	07.01.2020 08:05
	Turbulence	07.01.2020 07:19	07.01.2020 08:05
	Ozone	07.01.2020 07:19	07.01.2020 08:05
PS122/2_19-54	Tethersonde	08.01.2020 07:34	08.01.2020 09:35
	Turbulence	08.01.2020 07:34	08.01.2020 09:35
PS122/2_21-61	Tethersonde	22.01.2020 11:16	22.01.2020 12:12
	Ozone	22.01.2020 11:16	22.01.2020 12:12
PS122/2_21-62	Tethersonde	22.01.2020 13:01	22.01.2020 13:38
	Turbulence	22.01.2020 13:01	22.01.2020 13:38
	Ozone	22.01.2020 13:01	22.01.2020 13:38
PS122/2_21-119	Tethersonde	25.01.2020 07:26	25.01.2020 10:45
	Turbulence	25.01.2020 07:26	25.01.2020 10:45
	Filter Sampler	25.01.2020 07:26	25.01.2020 10:45
PS122/2_21-120	Tethersonde	25.01.2020 11:08	25.01.2020 11:58
	Turbulence	25.01.2020 11:08	25.01.2020 11:58
	Ozone	25.01.2020 11:08	25.01.2020 11:58
PS122/2_21-121	Tethersonde	25.01.2020 12:07	25.01.2020 12:37
	Turbulence	25.01.2020 12:07	25.01.2020 12:37
	Opt. particle	25.01.2020 12:07	25.01.2020 12:37
PS122/2_23-58	Tethersonde	06.02.2020 07:57	06.02.2020 10:04
	Turbulence	06.02.2020 07:57	06.02.2020 10:04

	Filter Sampler	06.02.2020 07:57	06.02.2020 10:04
PS122/2_23-59	Tethersonde	06.02.2020 11:19	06.02.2020 11:55
	Turbulence	06.02.2020 11:19	06.02.2020 11:55
	Filter Sampler	06.02.2020 11:19	06.02.2020 11:55
	Ozone	06.02.2020 11:19	06.02.2020 11:55
PS122/2_24-76	Tethersonde	15.02.2020 07:57	15.02.2020 10:26
	Turbulence	15.02.2020 07:57	15.02.2020 10:26
	Filter Sampler	15.02.2020 07:57	15.02.2020 10:26
PS122/2_24-77	Tethersonde	15.02.2020 10:44	15.02.2020 11:21
	Turbulence	15.02.2020 10:44	15.02.2020 11:21
	Opt. particle	15.02.2020 10:44	15.02.2020 11:21
	Ozone	15.02.2020 10:44	15.02.2020 11:21

- Eddy covariance and DTS system

The Eddy covariance system and the 10 m mast with the DTS glass fibre were build and installed during leg 2. The Eddy covariance system contains of a small weather hut, an Open Path Gas Analyzer from Licor for CO2 and H2O gas concentration, a Sonic Anemometer to measure all three wind components and the wind speed. With these data, the turbulent fluxes can be calculated. In addition, a camera is installed that takes a picture by movement and all 15 minutes. The whole system is installed on a Nansen sledge to have it mobile and movable with a snowmobile. First test measurements were performed 40 m northeast from BT. On January 23 2020, a 50 m wide lead opened approximately 1300 m from the ship. The mobile eddy system was transported there, measured and was evacuated on January 26 2020 after the lead formed to a ridge. Another lead opened near the Dark Site beginning of February and the eddy covariance system was measuring 3 days until the lead was completely frozen.

Because there were no other lead events, the eddy covariance system was established in MetCity mid-February to allow comparisons of the performance of different measurement systems and to compare the measurements performed with the same systems. In addition, a 10 m mast with the DTS glass fibre was installed next to the eddy covariance system at MetCity to generate a high resolution temperature profile.

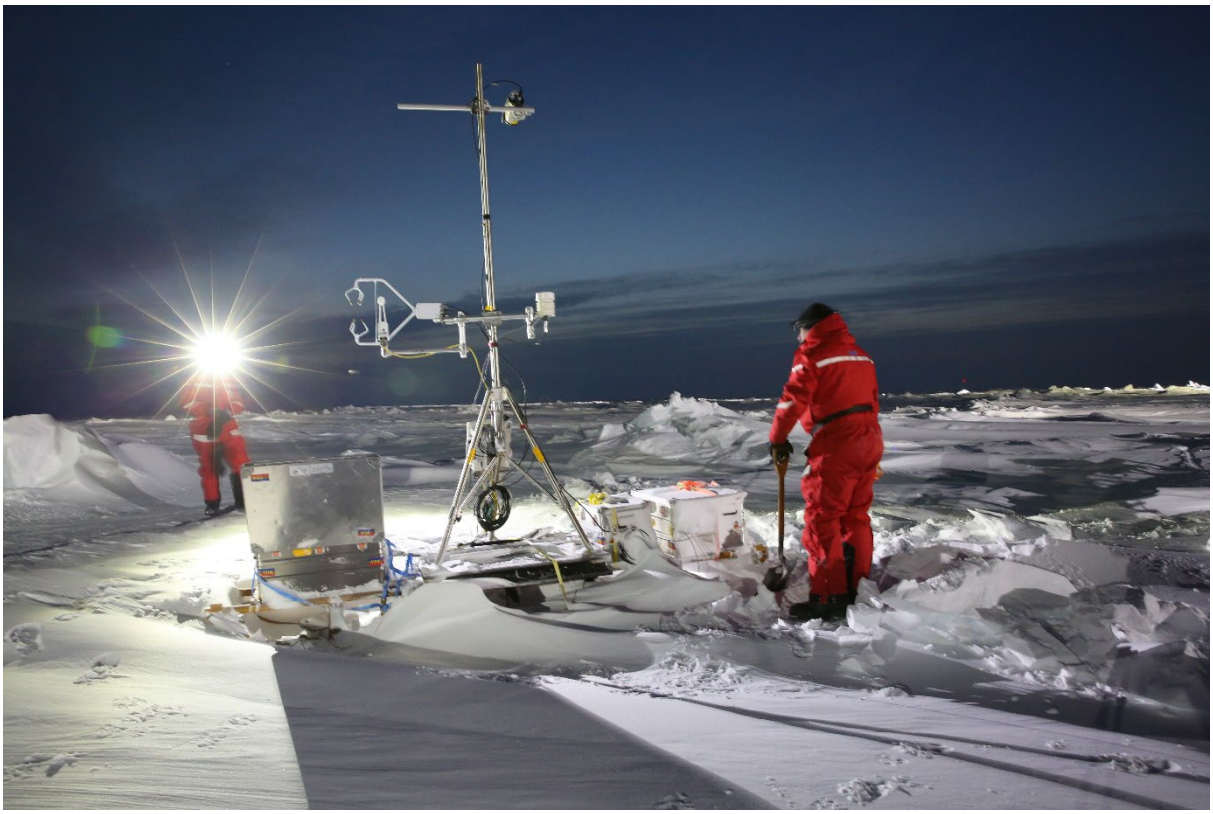

***Fig. 3.1.2**: Nansen sledge with Eddy covariance system in MetCity*

***Tab. 3.1.3**: List of all measurements performed with the eddy covariance system during Leg 2.*

Device operation	Position/Event	Start time UTC	End time UTC
PS122/2_20-54	Near BT – Eddy	16.01.2020 12:15	17.01.2020 11:25
PS122/2_20-102	Near BT – Eddy	18.01.2020 14:01	19.01.2020 11:00
PS122/2_21-83	Lead 1333 m from PS - Eddy	23.01.2020 13:18	26.01.2020 08:00
PS122/2_23-84	Lead at Dark Site – Eddy	04.02.2020 13:35	07.02.2020 12:15
PS122/2_24-103	MetCity	16.02.2020 14:01	17.02.2020 12:00
PS122/2_25-17	MetCity – Eddy	17.02.2020 12:18	22.02.2020 10:35
PS122/2_25-95	MetCity – Eddy	22.02.2020 12:13	26.02.2020 14:01
	MetCity – glass fibre	22.02.2020 11:58	24.02.2020 08:35

Preliminary (expected) results

The comprehensive record of radiosondes gives insight into the temporal evolution of meteorological key parameters over the atmospheric column from the near surface layers up to the stratosphere, and provides a linkage to larger-scale processes in the atmosphere. Measured parameters include temperature, relative humidity, wind speed and direction. The radiosonde measurements will directly used for the onboard weather forecast. Fig. 3.1.2 shows a sequence of temperatures and wind speeds as deduced from the soundings of leg 2. The temperature profiles indicate clearly the height of the tropopause around 9 km.

The profile of the wind speed show the polar vortex between 25 km and 30 km height. In addition, the storms that occurred in February 2020 are clearly visible in this plot. The phases with particular high wind speeds in the Troposphere are connected to the warm peaks with temperatures above -20°C.

Furthermore, the radiosonde data support the numerical weather forecast as observational input for the data assimilation.

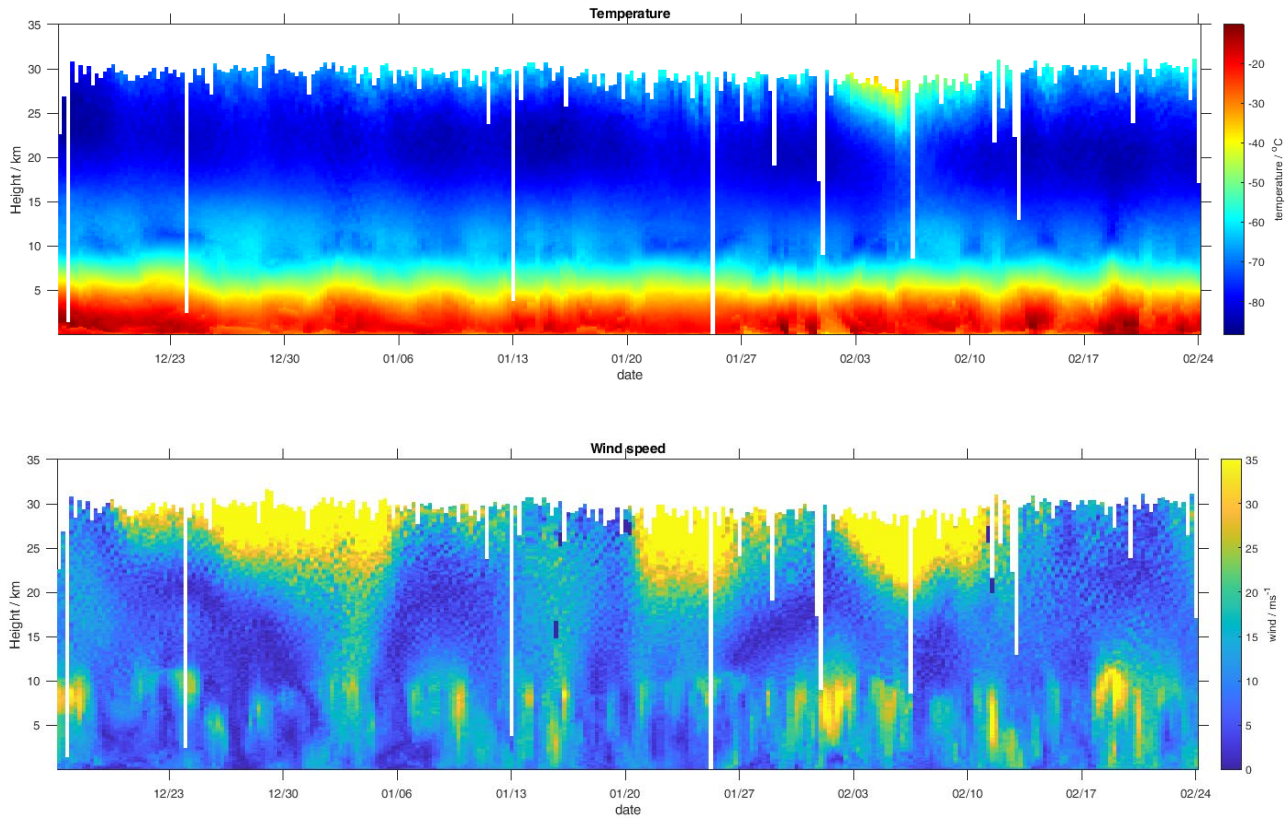

***Fig. 3.1.2**: time-height sections of temperature (top) and absolute wind speed (bottom) from leg 2 soundings.*

Data management

All data are handled, documented, archived and published following the MOSAiC data policy (see APPENDIX).

In addition, all radiosonde data have been transmitted to the GTS in near real-time to assure their availability for numerical weather forecast. All sounding data (radiosonde, ozone sonde, CFH, COBALD) and according auxiliary measurements are stored in the MCS. Upon the end of leg 2, the preliminary sounding data will be processed at the GRUAN Lead Centre in Lindenberg, Germany. The final sounding data will be made available via the PANGAEA data repository according to the MOSAiC Data Policy.

The DTS light backscatter profiles (incl. preliminary temperature profiles were also stored in the MCS after each measurement period. The final data processing of the DTS temperature profiles will be conducted at the Alfred Wegener Institute in Potsdam, Germany (contact: Alexander Schulz, alexander.schulz@awi.de). Final data products will be published via PANGAEA data repository according to the MOSAiC Data Policy as well.

References

Andreas EL, Paulson CA, William RM, Lindsay RW, Businger JA. 1979. The turbulent heat flux from arctic leads. Boundary-Layer Meteorol. 17, 57–91

Boé J, Hall A, Qu X (2009) Current GCMs' Unrealistic Negative Feedback in the Arctic. Journal of Climate, 22, 4682-4695

Graham R, Rinke A, Cohen L, Hudson SR, Walden VP, Granskog MA, Dorn W, Kayser M, and Maturilli M (2017) A comparison of the two Arctic atmospheric winter states observed during N-ICE2015 and SHEBA, J. Geophys. Res. Atmos., 122, 5716–5737

Holtslag AAM, Svensson G, Baas P, Basu S, Beare B, Beljaars ACM, Bosveld FC, Cuxart J, Lindvall J, Steeneveld GJ, Tjernström M, Van De Wiel BJH (2013) Stable Atmospheric Boundary Layers and Diurnal Cycles: Challenges for Weather and Climate Models. BAMS, 1691-1706

Inoue J, Yamazaki A, Ono J, Dethloff K, Maturilli M, Neuber R, Edwards P, and Yamaguchi H (2015) Additional Arctic observations improve weather and sea-ice forecasts for the Northern Sea Route, Science Reports, 5, 16868

Kayser M, Maturilli M, Graham RM, Hudson SR, Rinke A, Cohen L, Kim J-H, Park S-J, Moon W, Granskog, M (2017). Vertical thermodynamic structure of the troposphere during the Norwegian young sea ICE expedition (N-ICE2015). Journal of Geophysical Research: Atmospheres 122.20, 10855–10872.

Khaykin SM, Engel I, Vömel H, Formanyuk IM, Kivi R, Korshunov LI, Krämer M, Lykov AD, Meier S, Naebert T, Pitts MC, Santee ML, Spelten N, Wienhold FG, Yushkov VA, and Peter T (2013), Arctic stratospheric dehydration – Part 1: Unprecedented observation of vertical redistribution of water, Atmos. Chem. Phys., 13, 11503-11517

Maturilli M, and Dörnbrack A (2006) Polar stratospheric ice cloud above Spitsbergen, J. Geophys. Res., 111, D18210

Maturilli M, Fierli F, Yushkov V, Lukyanov A, Khaykin S, and Hauchecorne A (2006) Stratospheric Water vapour in the vicinity of the Arctic polar vortex. Annales Geophysicae, 24, 1511-1521

Manney GL, Santee ML, Rex M, Livesey NJ, Pitts MC, Veefkind P, Nash ER, Wohltmann I, Lehmann R, Froidevaux L, Poole LR, Schoeberl MR, Haffner DP, Davies J, Dorokhov V, Gernandt H, Johnson B, Kivi R, Kyrö E, Larsen N, Levelt PF, Makshtas A, McElroy CT, Nakajima H, Parrondo MC, Tarasick DW, von der Gathen P, Walker KA, and Zinoviev NS (2011) Unprecedented Arctic ozone loss in 2011, Nature, 478 (7370), pp. 469-475

Nash D, Waliser D, Guan B, Ye H, and Ralph F (2018) The role of atmospheric rivers in extratropical and polar hydroclimate, J. Geophys. Res. Atmos., 123, 6804–6821

Pavelsky TM, Boé J, Hall A, Fetzer, EJ (2011) Atmospheric inversion strength over polar oceans in winter regulated by sea ice. Climate Dynamics, 36, 945-955

Pithan F, Medeiros B, Mauritsen T (2014) Mixed-phase clouds cause climate model biases in Arctic wintertime temperature inversions. Climate Dynamics, 43, 289-303

Rex M, Harris NRP, von der Gathen P, Lehmann R, Braathen GO, Reimer E, Beck A, Chipperfield MR, Alfier R, Allaart M, O'Connor F, Dier H, Dorokhov V, Fast H, Gil M, Kyrö E, Litynska Z, Mikkelsen IS, Molyneux MG, Nakane H, Notholt J, Rummukainen M, Viatte P, and Wenger J (1997) Prolonged stratospheric ozone loss in the 1995/96 Arctic winter, Nature, 389 , pp. 835-838

Rex M, Salawitch RJ, von der Gathen P, Harris NRP, Chipperfield M, and Naujokat B (2004) Arctic ozone loss and climate change, Geophys. Res. Lett., 31, L04116

Rex, M, Salawitch RJ, Deckelmann H, von der Gathen P, Harris NRP, Chipperfield MP, Naujokat B, Reimer E, Allaart M, Andersen SB, Bevilacqua R, Braathen GO, Claude H, Davies J, De Backer H, Dier H, Dorokov V, Fast H, Gerding M, Hoppel K, Johnson B, Kyrö E, Litynska Z, Moore D, Nagai T, Parrondo MC, Risley D, Skrivankova P, Stübi R, Trepte C, Viatte P, and Zerefos C (2006) Arctic winter 2005: Implications for stratospheric ozone loss and climate change , Geophysical Research Letters, 33, L23808

Ruffieux D, Persson, POG, Fairall CW, Wolfe DE. 1995. Ice pack and lead surface energy budgets during LEADEX 1992. J. Geophys. Res. 100, 4593–4612

Sato K, Inoue J, Yamazaki A, Kim J-H, Maturilli M, Dethloff K, Hudson SR, and Granskog MA (2016) Improved forecasts of winter weather extremes over midlatitudes with extra Arctic observations, J. Geophys. Res. Oceans, 121

Sato K, Inoue J, Yamazaki A, Kim J-H, Makshtas A, Kustov V, Maturilli M, and Dethloff K (2018) Impact on predictability of tropical and mid-latitude cyclones by extra Arctic observations, Science Reports, 8, 12104

Stramler K, Genio ADD, and Rossow WB (2011) Synoptically driven Arctic winter states, Journal of Climate, 24(6), 1747–1762

Tetzlaff A, Lüpkes C, and Hartmann J (2015) Aircraft-based observations of atmospheric boundary-layer modification over Arctic leads, Quarterly Journal of the Royal Meteorological Society

Uttal, T, and Coauthors (2002): Surface heat budget of the Arctic Ocean. Bull. Amer. Meteor. Soc., 83, 255–275

von der Gathen P, Rex M, Harris NRP, Lucic D, Knudsen BM, Braathen GO, Backer HD, Fabian R, Fast H, Gil M, Kyrö E, Mikkelsen IS, Rummukainen M, Stähelin J, and Varotsos C (1995) Observational evidence for chemical ozone depletion over the Arctic in winter 1991-92, Nature, 375, pp. 131-134

Woods C, and Caballero R (2016) The role of moist intrusions in winter Arctic warming and sea ice decline, Journal of Climate, 29(12), 4473–4485

Yamazaki A, Inoue J, Dethloff K, Maturilli M, and König-Langlo G (2015) Impact of radiosonde observations on forecasting summertime Arctic cyclone formation, J. Geophys. Res. Atmos., 120

3.2 DOE ATMOSPHERIC RADIATION MEASUREMENT PROGRAM'S MOBILE FACILITY

Tercio Silva[3], Wesley King[3], Steele Griffiths[3]

(not on board:) Matthew Shupe[1,2], Heath Powers[3,4], Jim Mather[3,5], David Chu[3,4]

[1]EDU.CU
[2]GOV.NOAA
[3]GOV.ARM
[4]GOV.LANL
[5]GOV.SANDIA

Objectives

To understand the changing Arctic sea ice at a fundamental level requires a detailed accounting of energy flow through the sea ice system. While it is clear that atmospheric energy fluxes are critically important for the sea ice energy budget, many processes controlling these fluxes, and their interactions, are poorly understood and represented in numerical models. This project aims to observe specific processes that control the flow of energy through the Arctic atmospheric system and thereby to address pressing science questions under four broad topics.

(a) Surface Energy Budget: What is the annual evolution of the surface energy budget over young sea ice? What are the key process interactions determining the surface energy budget and specifically variability in surface radiation?

(b) Clouds and Precipitation: What factors determine Arctic cloud phase partitioning? What role do clouds and precipitation play in determining low-level atmospheric structure? How does surface inhomogeneity influence the spatial structure of cloud-precipitation systems?

(c) Aerosols: How do aerosol physical, chemical, and optical properties over sea ice vary seasonally? What sources and transport patterns are responsible for variability in Arctic aerosol? What are the radiative and cloud-nucleating properties of Arctic aerosol?

(d) Boundary Layer Structure: What are the properties and effects of stably stratified turbulence in the Arctic boundary layer? What are the effects of a thinned ice cover on boundary layer stability and heat fluxes? How do surface- and cloud-driven dynamics impact the boundary layer structure?

Work at sea

To provide the diverse and detailed atmospheric measurements needed to address the primary scientific objectives of the project, the US Department of Energy's Atmospheric Radiation Measurement (ARM) Program (www.arm.gov) has deployed its second ARM Mobile Facility (AMF-2) onboard and nearby *Polarstern* during MOSAiC. This extensive suite of instruments is operated in a collection of six laboratory sea-containers installed on the bow of *Polarstern*, one laboratory container installed on the *Polarstern* P-deck, as well as various instruments installed at Met City out on the sea ice of the Central Observatory. ARM has also provided funding support for one half of the meteorological radiosonde program led by AWI during MOSAiC, as well as personnel support for launching some of these soundings. The AMF-2 facility can be described via five instrument collections, which are captured in Table 3.2.1.

Tab. 3.2.1. All instruments installed and operated by the DOE ARM program, including the measurement objectives, installation location, and start date for observations.

Instrument	**Measurement Objectives**	**Installation Location**	**Start of Observations**
Meteorology and Winds			
Radiosonde Program (support for ½ of equipment)	Profiles of temperature and humidity	Helideck	20 Sept
Present Weather Detector (PWD)	Visibility	(1) P-deck port side; (2) Met City	17 Oct
Beam-steerable radar wind profiler (BSRWP)	Wind profiles	KAZR lab (C3)	5 Oct
Doppler lidar (DL)	Wind profiles, turbulence	Top OPS lab (C4)	7 Oct
Cloud Properties and Processes			
2-channel microwave radiometer (MWR2C)	Liquid water path and precipitable water vapor	Lower P-deck port side	16 Oct
3-channel microwave radiometer (MWR3C)	Liquid water path and precipitable water vapor	Lower P-deck port side	8 Oct
Ka-Band ARM Zenith Radar (KAZR)	Cloud occurrence and properties	KAZR lab (C3)	5 Oct
Marine W-Band ARM Cloud Radar (MWACR)	Cloud occurrence and properties	Top of OPS lab (C4)	16 Oct
High Spectral Resolution Lidar (HSRL)	Cloud & aerosol properties	OPS lab (C4)	10 Oct
Micropulse Lidar (MPL)	Cloud & aerosol properties	OPS lab (C4)	5 Oct
Ceilometer (CEIL)	Cloud base height	Lower P-deck port side	8 Oct
Total Sky Imager (TSI)	Hemispheric sky views	P-deck	Not installed yet
Precipitation			
Ka-Band Scanning ARM Cloud Radar (Ka-SACR)	Cloud and precipitation spatial distribution	P-deck, starboard side	5 Oct
Parsivel2 Laser Disdrometer (LDIS)	Fall velocity and precipitation rate of precipitation	(1)P-deck port side; (2)Met City double Altar shield	(1) 30 Oct, (2) 14 Nov

Pluvio2 Weighing Bucket Rain Gauge (WBRG)	Precipitation mass	Met City in double Altar shield	30 Oct
Siphon Rain Gauge (SRG)	Precipitation mass	P-deck port side	30 Oct
Radiation			
Marine Atmospheric Emitted Radiance Interferometer (MAERI)	Spectral infrared radiation, both downwelling and upwelling	Lower P-deck port side, view to port side ice	9 Oct
Cimel Sunphotometer (CSPHOT)	Atmospheric transmission & scattering during daylight	P-deck	Not yet installed
Fast Rotating Shadowband Radiometer (FRSR)	Direct and diffuse components of downward solar flux	P-deck	14 Oct
Ground Radiometer System (GNDRAD) – PIR, PSP	Upwelling shortwave and longwave radiation	Met City "swingset"	14 Oct
Ground Infrared Thermometer (IRT)	Ground temperature with wide field-of-view	Met City "swingset"	30 Oct
Multifilter Radiometer 3-meter (MRF3M)	Reflected radiative flux in narrow bands	Met City "swingset"	14 Oct
Ice Radiometer System (ICERAD) – PIR, PSP, SPN1	Downwelling shortwave and longwave radiation, with shortwave direct and diffuse	Met City	14 Oct
Shipboard Radiometer System (SHIPRAD) – PIR, PSP, SPN1	Downwelling shortwave and longwave radiation, with shortwave direct and diffuse	(1) P-deck port side; (2) P-deck starboard side	(1) 7 Oct; (2) 7 Oct
Sky Infrared Thermometer (IRT)	Sky temperature with narrow field-of-view	Met City "swingset"	14 Oct
Aerosols and Gases			
Automated Weather Station (AOSMET)	Pressure, temperature, relative humidity, winds	AOS inlet on AOS lab (C5)	9 Oct
Trace Gas Monitors	Concentrations: carbon monoxide, nitrous oxide, water vapor	AOS lab (C5)	9 Oct
Ozone Monitor	Concentration of ozone	AOS lab (C5)	9 Oct
Aerosol Chemical Speciation Monitor (ACSM)	Bulk chemical composition	AOS lab (C5)	8 Nov
Condensation Particle Counter (CPC)	Total particle concentration for sizes >10nm	AOS lab (C5)	8 Oct
Ultrafine Condensation Particle Counter (UCPC)	Total particle concentration for sizes >3nm	AOS lab (C5)	8 Oct
Cloud Condensation Nuclei Counter (CCN)	Concentration of cloud condensation nuclei	AOS lab (C5)	8 Nov
Scanning Mobility Particle Sizer (SMPS)	Aerosol size distribution	AOS lab (C5)	9 Oct

Ultra-High Sensitivity Aerosol Spectrometer (UHSAS)	Aerosol size distribution	AOS lab (C5)	7 Oct
Humidified Tandem Differential Mobility Analyzer (HTDMA)	Aerosol size distribution exposed to different moisture levels	AOS lab (C5)	28 Sept
Single Particle Soot Photometer (SP2)	Soot mass of aerosol particles	AOS lab (C5)	15 Oct
Particle Soot Absorption Photometer (PSAP)	Bulk aerosol absorption	AOS lab (C5)	8 Oct
Nephelometer (NEPH)	Total aerosol scattering at 450, 550, and 700 nm wavelengths	AOS lab (C5)	8 Oct

In addition to the core AMF-2 instruments, ARM has agreed via a proposal process to host and operate instrumentation for two collaborating scientists, Drs. Jessie Creamean and Kerri Pratt. These guest instruments complement the core ARM measurements by the addition of ice nucleus filters, drum samplers, and impactors, all sampling off of the Aerosol Observing System's inlet.

The ARM facility was supported on MOSAiC Leg 2 by 3 on-site technicians (Silva, Griffiths, King).

Operations during Leg 2 were generally robust, with the following issues.

- The X-band Scanning ARM Cloud Radar (X-SACR) system never operated robustly in spite of many attempts to replace, fix, or modify different components; thus, the only scanning radar system available is the Ka-band component of the SACR.
- The AOS system samples air through an inlet and has a special design to minimize sampling of ship's exhaust; this includes monitoring parameters like carbon monoxide to trigger a back flow through the stack during periods of pollution. Thus, for certain periods, typically determined by wind direction, aerosol sampling was not possible.
- The Humidified Tandem Differential Mobility Analyzer (HTDMA) had a problem with the drain system during Leg2, waiting spares will come for Leg4.
- The Multifilter Radiometer 3-meter (MRF3M) had a problem since the begin of the campaign, after receiving the spare board (at the end of Leg2) and repaired some connectors at the logger, instrument is working properly now.

Preliminary (expected) results

Primary results from the AMF-2 deployment at MOSAiC will be an extensive collection of high-quality data sets from the AMF-2 instrumentation that are as continuous as possible for the full year. These data sets will be quality assured by a large team of instrument mentors and facility managers that will not participate in the field at MOSAiC. Based on these data sets, a suite of value-added products will also be derived to provide information on geophysical parameters related to the atmospheric state, clouds, aerosols, vertical atmospheric structure, and others. These data sets are intended to support a great deal of process-based research in support of advancing knowledge, assessing models, and developing improved models for representing climate processes.

Data management

All data are handled, documented, archived and published following the MOSAiC data policy (see APPENDIX). In addition, all data produced by the ARM Program during MOSAiC Leg 2

has been automatically ingested and stored on ARM's onboard "site data system," which performs many operational tasks involved with data management, initial data ingesting and formatting, data quality checks, and the production of quicklook plots of the data. Quicklooks are available via a web page to other scientists onboard *Polarstern* (https://192.168.3.33:8443) and to the general public (https://dq-amfc2.amf.arm.gov). With nearly 32 TB of data produced during Leg 2, it has been agreed that this data will not initially be uploaded to the MOSAiC Central Server, however, MOSAiC scientists can get access to the raw data through a free account on ARM's site data system (192.168.3.33:22) by obtaining credentials from the ARM data manager (see ARM technicians onsite). After MOSAiC Leg 1, and all subsequent legs, the full set of collected data are physically transported to the ARM data management facility and promptly ingested into a full set of processed data files that will then be publicly available via the ARM Data Archive (www.archive.arm.gov). Raw data will be available within a couple of weeks of its arrival at the data management facility. Based on this raw data, a suite of value-added products will also be developed in the following months, with these products also being served at the ARM Archive. Appropriate meta-data sharing and cross-linking will occur via the MOSAiC Central Storage and with PANGAEA (World Data Center PANGAEA Data Publisher for Earth & Environmental Science (www.pangaea.de)) according to the protocol agreed upon between these two archives.

References

None

3.3 TROPOS – OCEANET: REMOTE SENSING OF THE ANNUAL CYCLE OF AEROSOL, CLOUD, AND CORRESPONDING RADIATION CLOSURE STUDIES IN THE CENTRAL ARCTIC

Hannes Griesche[1],

(not on board:) Ronny Engelmann[1], Martin Radenz[1], Julian Hofer[1], Dietrich Althausen[1], Holger Baars[1], Patric Seifert[1], Albert Ansmann[1], Andreas Macke[1], Mario Mech[2], Bernhard Pospichal[2], Kerstin Ebell[2], Susanne Crewell[2], Gaël Dubois[3], Luc Blarel[3], Philippe Goloub[3]

[1]DE.TROPOS

[2]DE.UNI-KOELN

[3]FR.UNIV-LILLE

Objectives

Measurements of the atmospheric state in the Arctic are extremely rare and of great interest for climate research in this unique and changing environment. The mobile facility OCEANET is an ongoing observational initiative of TROPOS for aerosol and cloud profiling as well as radiation budget measurements in maritime environments onboard research vessels since 2007 (Kanitz et al., 2013, Bohlmann et al., 2018). One of the key focusses for TROPOS lies on heterogeneous ice formation processes in different areas of the world (e.g., Kanitz et al, 2011) and their radiative impact. During MOSAiC PS122/2 the OCEANET state-of-the-art en-route measurements were implemented on *Polarstern* in order to establish a full Arctic annual aerosol, cloud, and radiation data record.

The following research question are addressed within this project:

- How do aerosol- and cloud properties influence the annual cycle of short-wave and long-wave radiation under different meteorological conditions in the Arctic?
- How often does ice formation in warm (T > –10 °C) stratus clouds occur and what are possible freezing mechanisms under clean Arctic conditions?
- Can we observe different ice-formation rates in the presence of local and long-range transported ice nucleating particles?
- Will Arctic clouds increase or suppress the currently observed Arctic warming?
-

An additional focus is on ESA's Aeolus wind mission. OCEANET data will also support the CAL/VAL activities of this lidar satellite within the EVAA project. Since it is a polar-orbiting satellite, a large number of overpasses in the close vicinity of *Polarstern* occurred during PS122/2.

Work at sea

The OCEANET container of TROPOS was already installed on the bow of *Polarstern* at the container location C8 during MOSAiC Leg 1.

Since then continuous measurements with the

- the multi-wavelength Raman depolarization lidar Polly-XT (Engelmann et al., 2016),
- the microwave radiometers HATPRO and LHUMPRO,
- the CIMEL sun/sky/lunar photometer (Yin et al., 2019),
- two disdrometers, Parsivel² and 2DVD,
- a total-sky imager,
- a pyranometer and a pyrgeometer,
- and a basic DWD weather station (T,p,r.h.)

were performed.

During the cruise all instruments had to be monitored for operation and several maintenance and calibration tasks were performed. For example, the laser of Polly-XT, needed a flash lamp replacement which resulted in a technical downtime of about 4 hours for the lidar. Additional periods with no lidar operation were mainly caused by crane operations above the OCEANET container as well as helicopter operations with direct overflies over the lidar. In Figure 3.3.1 the position of the OCEANET platform at the bow of *Polarstern* is shown.

Fig. 3.3.1: View from the bow crane on the OCEANET container (left) in front of the bridge of *Polarstern*. On the right hand side the KAZR on top of the ARM Radar container is partly visible.

At the beginning of Leg 2 and during the changeover to Leg 3 the microwave radiometers were calibrated with liquid nitrogen. It was known, that the LN2 generated on board would contain a certain percentage of oxygen and thus the boiling temperature would be different depending on the purity. Hence, the temperature of the LN2 was determined with a designated thermometer. Instead of 77.14 K of pure LN2 a temperature of 77.89 K was determined and used for the calibration procedure.

The sun/sky/lunar CIMEL photometer could only operate as soon as the moon was above the horizon, visible for the photometer from its location on the foredeck container, and the sky was free of clouds. The robot of the CIMEL photometer, which should point the photometer towards the moon, had occasionally appearing malfunctions. Despite all the efforts taken to fix these problems, with the remote support of the engineers from the University of Lille, no completely reliable performance of the robot could be archived. Nevertheless, measurements were still possible during several days during Leg 2.

The pyranometer and pyrgeometer were installed on the bow-crane. This location seemed the most favorable to avoid shading by the ships superstructure.

In addition to the technical setup and maintenance of the OCEANET instrumentation an automatic profile retrieval algorithm for Polly-XT (Picasso) was operated to observe online data and aerosol profiles. This automatic dataset will be reanalyzed later according to PollyNET standards (Baars et al., 2016).

One of the main goals of this project is to link the aerosol information to cloud structure and radiative effects. For this purpose, we could make use of the preliminary data from the ARM KAZR cloud radar, the regular radiosoundings on board, and from the OCEANET lidar and microwave radiometer data and implement the Cloudnet algorithms (Illingworth et al., 2007). In this way, synergistic products could already be derived shortly after the measurements which can be accessed online within *Polarstern's* internal network.

Preliminary (expected) results

During PS122/2 aerosol layers up to heights of 15 km were observed regularly with the multi-wavelength Raman Lidar Polly-XT. In Figure 3.3.2 the 1064-nm range-corrected lidar signal on 4 February 2020 is shown. Besides backscattering from aerosols closer to the ground up

to 3 km height there were several stratified layers visible especially at 4-6 and 9-15 km height. The stratospheric layer was visible in all cloud-free profiles during the entire Leg 2 (see Figure 3.3.3). Further in-depth analysis of the optical properties is required, but from first analysis it can be stated, that these are most likely highly absorbing pollution aerosols either from the long-ongoing Arctic fires in 2019 or from mid-latitude continental sources.

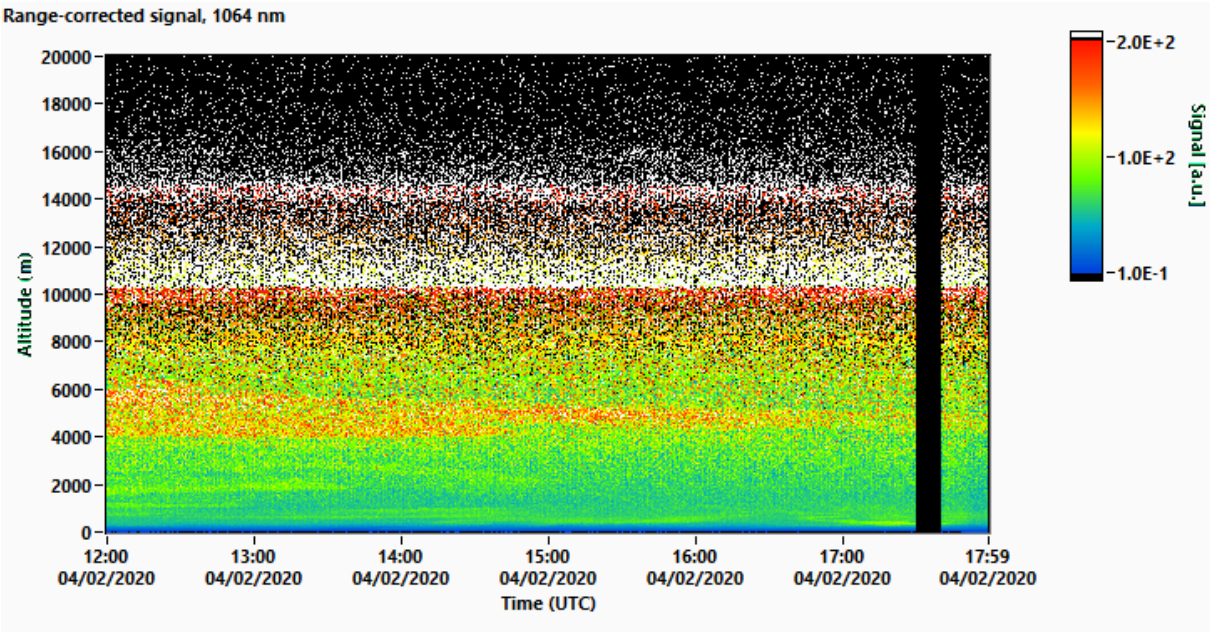

Fig. 3.3.2: Range-corrected lidar signal at 1064 nm on 4 February 2020.

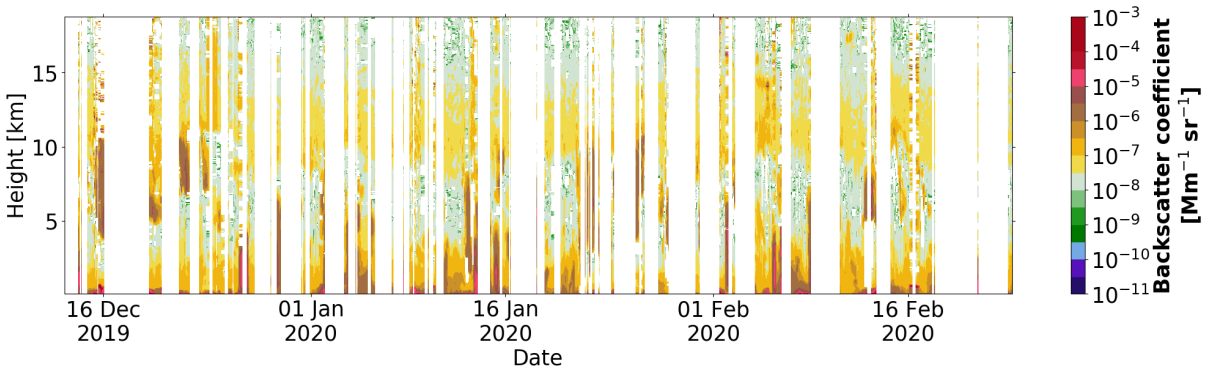

Fig. 3.3.3: Contour plot of all retrieved backscatter coefficient profiles from the automatic profile retrieval algorithm Picasso during Leg 2 from 13 December 2019 until 24 February 2020. Periods with missing data are mostly due to signal attenuation because of low-level clouds or blowing ice crystals or helicopter and crane operations.

The lidar Polly-XT is also equipped with a Raman channel for the detection of water vapor. In a combination with the temperature profiles from the regular *Polarstern* radiosoundings it was possible to derive profiles of relative humidity on a few-minutes resolution on the assumption that the variability of the water vapor drives the relative humidity while the temperature profiles in greater altitudes changes much slower (Guangyao et al., 2018). Such profiles like presented in Figure 3.3.4 for 4 February 2020 will be a good additional source for in-depth cloud analysis later on.

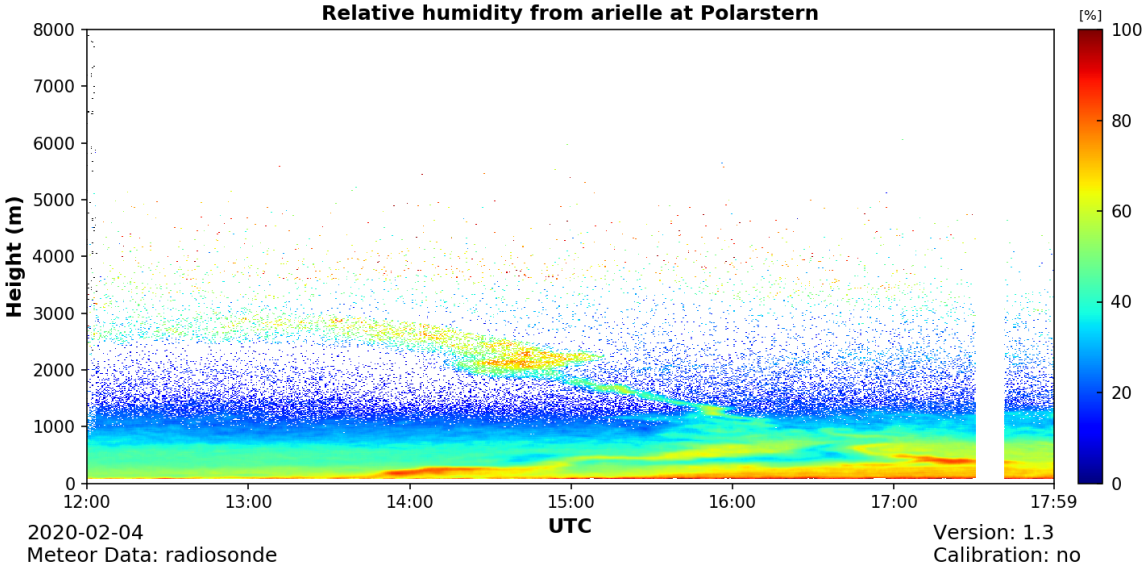

Fig. 3.3.4: Relative humidity derived from Polly-XT with the assumption of a constant temperature profile from the 6-h radiosonde on 4 February 2020.

Additional to the lidar, the OCEANET platform also operated two microwave radiometers, one HATPRO from TROPOS and one LHUMPRO from the University of Cologne. The latter one measures at higher frequencies at which the water-vapor absorption coefficients are stronger, so that it can give better estimates for integrated water vapor and liquid-water path for thin Arctic stratus clouds. For denser cloud systems however, the signals will saturate quickly. Therefore, we employed the combination of both systems to be able to give a full time series of IVW and LWP.

For the first time in the Central Arctic winter we operated a shipborne AERONET sun/sky/lunar Cimel Photometer from the University of Lille. Figure 3.3.5 shows the very first analysis of the Aerosol Optical Depth (AOD) for the moon phase in December 2019 at six different wavelengths and the precipitable water.

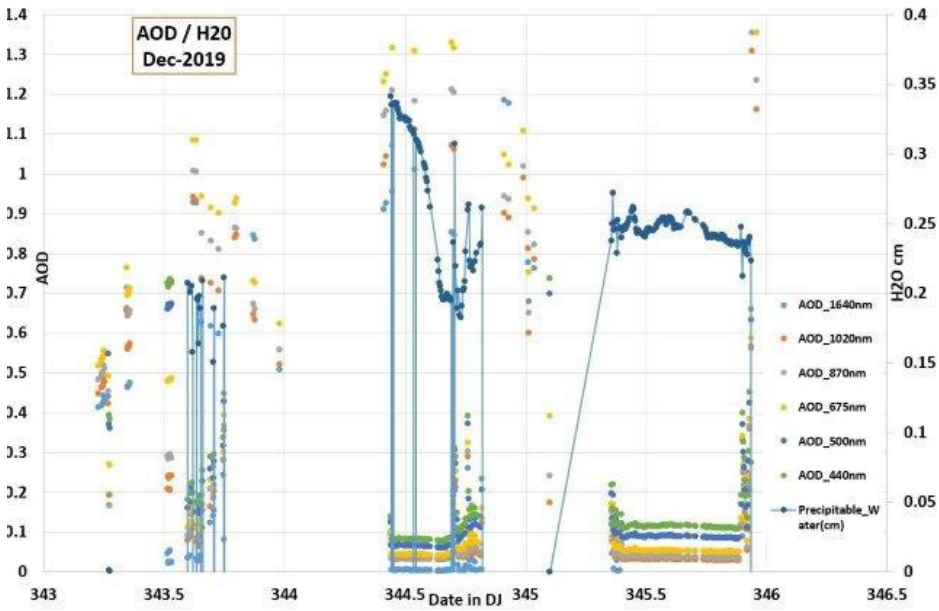

Fig. 3.3.5: First preliminary data from the shipborne Lunar Photometer at the Central Arctic. Aerosol Optical Depth vs. time in December 2019.

For MOSAiC we implemented the *Cloudnet* software package at the server system of the OCEANET platform and integrated the preliminary ARM KAZR data (section 3.2), together with the regular 6h radiosounding program (section 3.1), and the Polly-XT lidar to derive synergistic products. Figure 3.3.6 shows an example of the target classification product, and the ice-particle effective radius from this integrated dataset on 17 February 2020.

During Leg 2 we usually observed pure ice clouds that occasionally contained liquid-water patches or status liquid-water layers (e.g. from 15 – 20 UTC in Fig. 3.3.6) that immediately started nucleation of ice particles and formed ice-particle virgae. The purpose of this early stage of synergistic retrieval was to be able to lively track the current atmospheric observations. Careful post- and reprocessing of these datasets are however needed, once the data went through their individual QA/QC and publication routines.

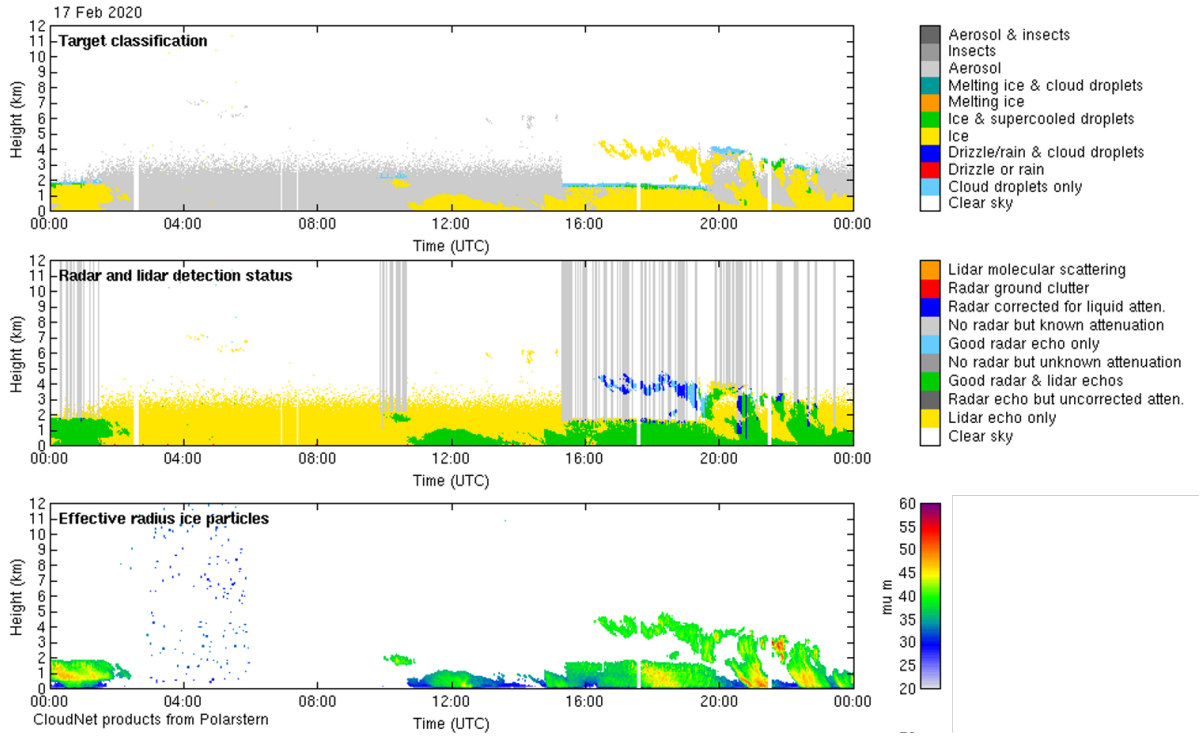

Fig. 3.3.6: Some selected Cloudnet products (target classification, detection status, and effective radius of ice particles) automatically generated during Leg 2 on 17 Feburary 2020.

Data management

All data are handled, documented, archived and published following the MOSAiC data policy (see APPENDIX). In addition, the Polly-XT lidar data and quicklooks will be processed and made available through PollyNET (http://polly.tropos.de). After final processing the other individual datasets will be published within PANGAEA.

References

Baars, H. et al. (2016) An overview of the first decade of PollyNET: an emerging network of automated Raman-polarization lidars for continuous aerosol profiling, Atmos. Chem. Phys., 16, 5111–5137.

Bohlmann, S. et al. (2018) Ship-borne aerosol profiling with lidar over the Atlantic Ocean: from pure marine conditions to complex dust–smoke mixtures, Atmos. Chem. Phys., 18, 9661–9679.

Engelmann, R. et al. (2016) The automated multiwavelength Raman polarization and water-vapor lidar PollyXT: the neXT generation, Atmos. Meas. Tech., 9, 1767–1784.

Guangyao D. et al. (2018) Calibration of Raman lidar water vapor profiles by means of AERONET photometer observations and GDAS meteorological data, Atmos. Meas. Tech., 11, 2735-2748.

Illingworth, A.J. et al. (2007) CloudNet: Continuous evaluations of cloud profiles in seven operational models using ground-based observations, Bull. Amer. Meteor. Soc., 88, 883-898.

Kanitz, T. et al. (2013) North-south cross sections of the vertical aerosol distribution over the Atlantic Ocean from multiwavelength Raman/polarization lidar during Polarstern cruises, J. Geophys. Res. Atmos., 118, 2643-2655.

Kanitz, T. et al. (2011) Contrasting the impact of aerosols at northern and southern midlatitudes on heterogeneous ice formation, Geophys. Res. Lett., 38, L17802.

Yin, Z. et al. (2019) Aerosol measurements with shipborne sun-sky-lunar photometer and collocated multiwavelength Raman polarization lidar over the Atlantic Ocean, Atmos. Meas. Tech., in press.

3.4. ATMOSPHERIC SURFACE FLUXES FOR UNDERSTANDING SEA-ICE THERMODYNAMICS AND DYNAMICS

Taneil Uttal[1,2], Michael Gallagher[1,2]

(not on board:) Matthew Shupe, Ola Persson, David Costa, Ian Brooks, Thomas Ayers[2], Christopher Cox[2], Christopher Fairall[2], Daniel Gottas[2], Jesse Leach[2], Sara Morris[2], Jackson Osborn[1,2], Sergio Pezoa[2], Jennifer Hutchings[4], Don Perovich[5], Timothy Stanton[6], Roberta Pirazzini[7]

[1]EDU.CU
[2]GOV.NOAA
[3]UK.UNI-LEEDS
[4]EDU.ORSU
[5]EDU.DARTMOUTH
[6]EDU.NPS
[7]FI.FMI

Objectives:

This project is designed to examine the Surface Energy Budget (SEB) and how it impacts the sea-ice thermodynamic and dynamic processes that control the state of the ice over a full year. The PS122/2 collection period was during the Arctic winter which is arguably the least documented and understood part of the annual cycle for the individual radiative, turbulent and conductive flux components of the SEB. In combination with partner MOSAiC projects, the overarching project objectives include:

(a) Build comprehensive atmospheric SEB, sea ice energy, upper ocean heat, and sea-ice momentum budgets; examine how these co-vary in space and time over all seasons of the year; and develop temporally-evolving process relationships among multiple key parameters.

(b) Use detailed field observations and a coupled regional model to examine how energy transfer processes (thermodynamics) are influenced by sea-ice deformation (dynamics) on sub-seasonal to seasonal time scales.

(c) Assess sea-ice predictability related to dynamic and thermodynamic process relationships, using a full year of quasi-operational, 10-day sea-ice forecasts.

In support of these broad project goals, the specific objectives of the SEB Flux team during PS122/2 was to continue operation of the SEB flux and related measurement systems deployed during PS122/1 as well as provide operational support for a number of related guest programs that did not have representatives on-board during PS122/2. A more detailed description of the SEB Flux project objectives can be found in the PS122/1 cruise report and are not repeated here.

This project is funded by the US National Science Foundation and the US National Oceanic and Atmospheric Administration.

Work at Sea

Tasks for the PS122/2 SEB Flux Team had 3 components: Maintenance of the 11 m tower at Met City, maintenance of Automated Surface Flux Stations (ASFSs) at the 3 L-sites in the Distributed Observatory and maintenance of a number of partner programs at both Met City and on the *Polarstern.*

Met City

Although the arrival of the Kapitan Dranitsyn in combination with tidal forces during a full moon phase appeared to precipitate new cracks (up to 2 m wide) in the in the vicinity of Met City around December 13th, these refroze quickly and did not impact operations for the duration of PS122/2. During PS122/1 the 11 m tower was originally located so that it was the furthest installation from *Polarstern* with most other activities in the MOSAiC Central Observatory being installed in an approximately linear arrangement back in the direction of *Polarstern*. This installation plan was conceived to accommodate the heat and momentum flux calculations measured by the 11 m tower by minimizing the wind sector that would be adversely impacted by other installations and to have a measurement footprint that is as representative as possible of the regional ice conditions. This careful planning during PS122/1 went astray during a major rearrangement of the floe on 16-22 November during which episodic rapid ice movement changed the configuration of the Central Observatory, moving Met City forward of the bow of the *Polarstern* and to a range of less than 350 m. Therefore, PS122/2 inherited a significantly changed measurement environment with new sectors in which there were artificial roughness elements, in particular the *Polarstern*. Met City site during PS122/2 had significant natural ridging around 12 m tower in all quadrants and a number of events in February (dates?) further evolved the topography around the site with accumulations from blowing snow and average site snow depth was estimated to increase from 15-20 cm to 60-70 cm. A number of installations (buoys) were buried, some end up at the bottom of snow wells (AOFB and Met Hut) and some sensors became positioned significantly closer to the surface (IRT and SR50, VISSS and FMI radiation) and in general, by the end of PS122/2, ridged regions around Met City became generally flatter. The base of the 11 m tower stayed clear and there were no major snow removal activities with the exception of keeping the data logging boxes clear of snow. Figure 3.4.1 shows the extended region around Met City viewed with the ALS system on Feb 25.

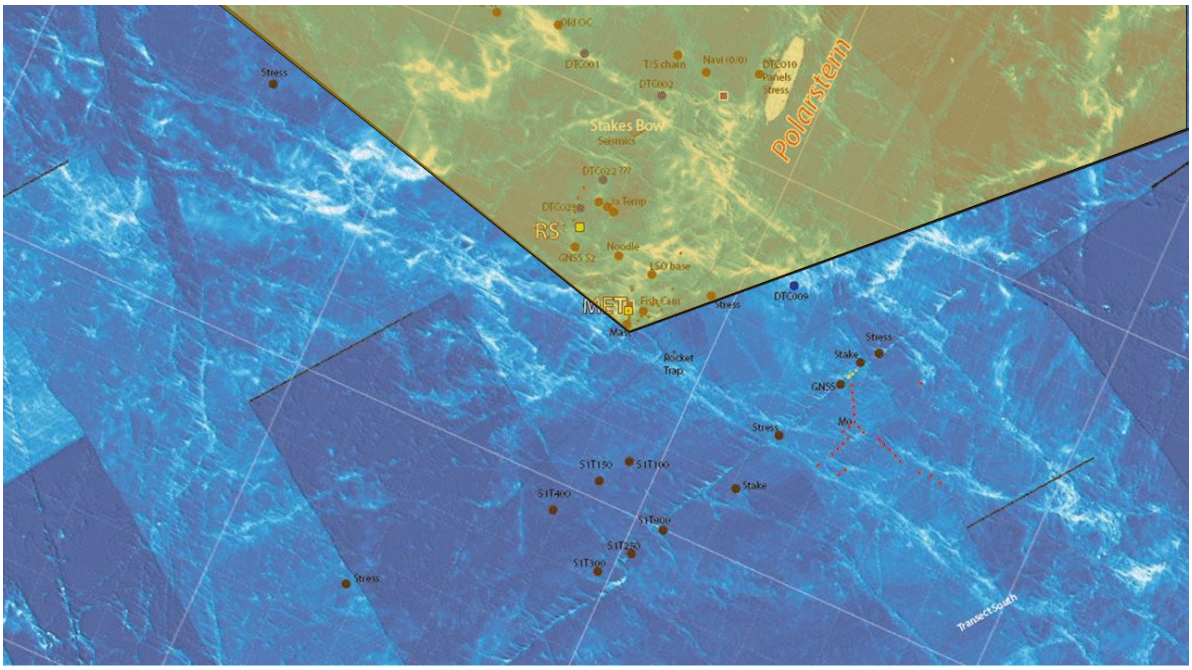

Figure 3.4.1 Extented area around the Met City SEB 11 meter flux tower from the Feb 21 ALS scan. The region with probable artificial disturbance of turbulence measurements is in the shaded area. The remaining installations (e.g. SIT sites)

on the figure were part of transect zones with records of now depth, ice thickness and a proxy measurement for snow density. The companion TLS scans for the Snow1 area will be useful for the FLUX SEB project, especially for characterizing surface roughness.

Another Met City site feature that had some potential for impacting turbulent and radiative flux calculations was the installation of 3 light posts to replace the usage of trip wires on the southern border of the CO; The light posts were carefully positioned to not influence any of the SW radiometers operated by ARM and FMI however one was between the 11 m tower and Snow 1. It should also be noted that and the ship search lights were frequently positioned on Met City either by request while working on site or for general surveillance (Fig 3.4.2).

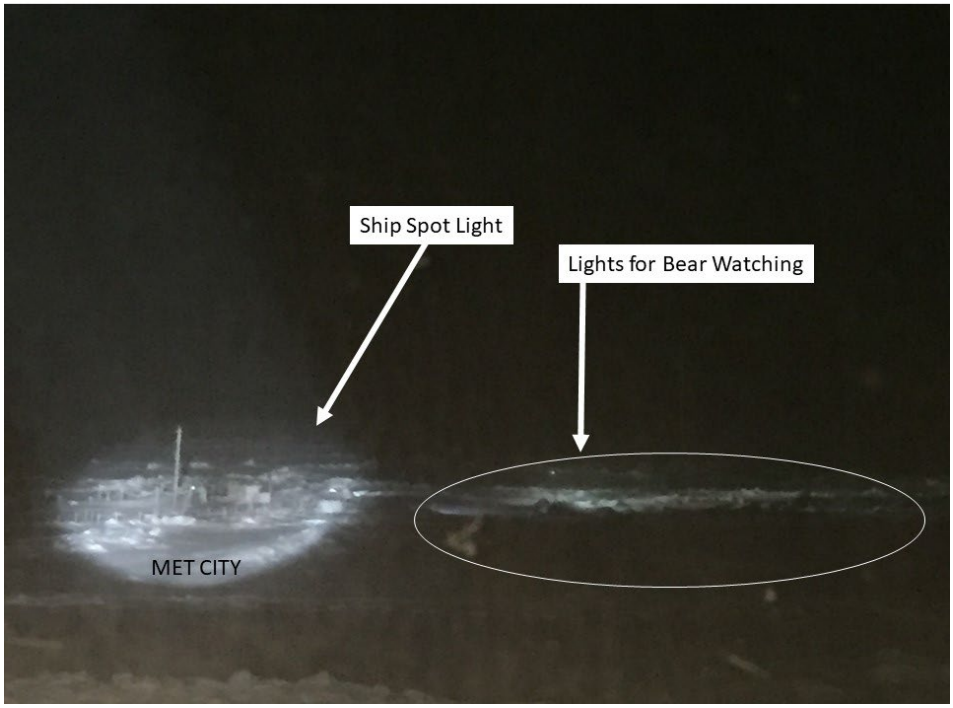

Figure 3.4.2 Light pollution around Met City during PS122/2

New waypoints were measured on February 12, 2020 and these were registered on the February 21 ALS scan (Figure 3.4.3). Near daily checks by the SEB Flux team at Met City included removing snow and ice from the 2 meter level sensors, the VISSS and FMI radiometers; trips to Met City were made in partnership with the ARM team that monitored the operation of the additional met sensors. The Licor instrument for measuring CO2 and H2O and the FMI radiometers were particularly impacted by riming, however there were several extended periods when environmental conditions (high winds) resulted in these instruments being naturally “cleaned”. The 11 m tower (Figure 3.4.4) was the platform for a number of additional instruments from partner observing programs (BAS) including an Optical Particle Spectrometer (CLASP) for measuring aerosol size distributions that was installed initially at 3 m and two snow particle counters (SPCs) originally at ~0.5 and 10 m heights. Instructions were left to raise the lower SPC in the event that it reached within 0.1 m. It was about at this level as the Leg III BAS representative arrived on site. The CLASP was also found to occasionally and expectedly become obstructed by snow which was cleaned manually. The SEB Flux team also did occasional checks (turning the inlets into the incoming wind) and collections from the rocket traps in Snow 1 (Fig 3.4.6) and physically maintained the 23 m mast (Figure 3.4.7 a and b); this entailed keeping the guy lines, data and power cables above the snow and drift levels and on one occasion adjusting the cabling. Because of the dark, it was not possible to effectively re-verify the orientation of the mast relative to the tower, however, because of the local floe stability during PS122/2 it is assumed that for processing purposes that the relative orientation of the tower and the mast did not change. The SEB Flux team also removed drifts

and snow from around and in the enclosure around the SODAR which became increasingly frequent and severe as PS122/2 progressed (Figure 3.4.6). The SODAR was the one instrument with extended data outage periods (see Table 3.4.1); this occurred due an Arctic Fox chewing through communication cables to Met City.

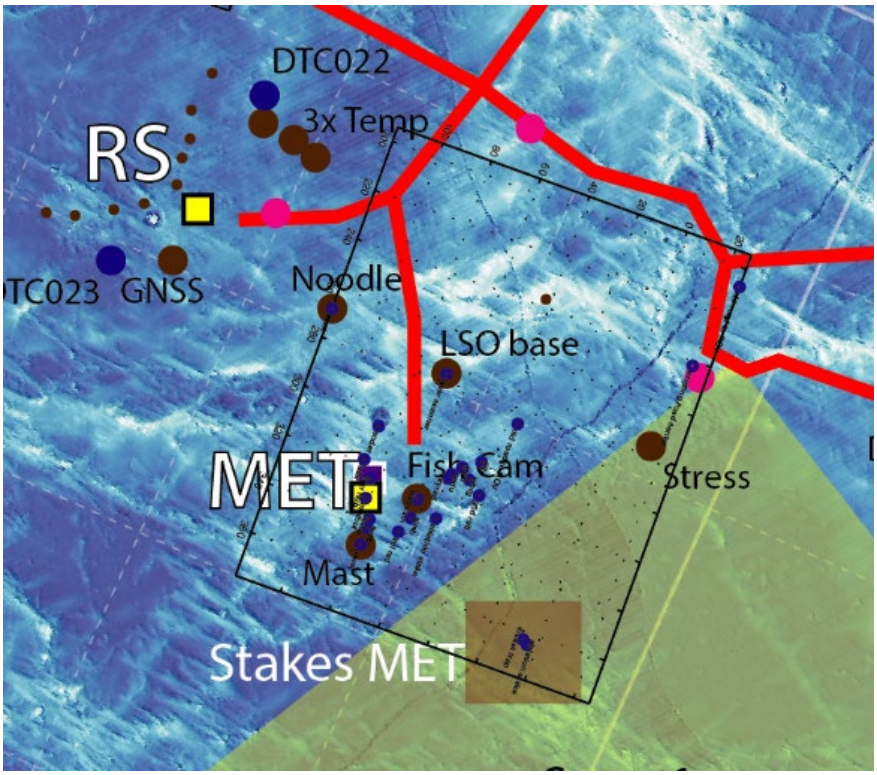

Figure 3.4.3 – Locations of major MET CITY installations. Waypoints from Feb 12, ALS scan from Feb21.

Figure 3.4.4 – 11 m Flux Tower being cleaned of snow and ice accumulation of Feb xx. (Photo Credit: Taneil Uttal)

Platform	Variables	Notes	Data Recovery
11 m tower (ice-snow interface)	Conductive flux	The 11 m tower and 23 m mast operated almost continuously for the entire official	X%

11 m tower (2 m)	u, v, w, T, RH, P, Hdg, Lat, Lon, Sfc Temp, CO_2, H_20	period of Leg 2 (December 15, 2019 to February 22, 2020). There was brief power outage on XX. A second ship-wide power outage on XX resulted in a XX hour gap. There were 2 communications outages on XX and XX. These did not affect operations and data was recovered manually	
11 m met tower (6m, 11m)	u, v, w, T, RH		
Mast (23 m)	u, v, w, T, RH, P		
SODAR		An Arctic fox chewed the communication cables to Met City. This caused a SODAR data outage from xx to xx.	X%
Lidar – Met City	u, v, w up to 1000m		
Lidar - Ship	u, v, w up to 1000m		
FMI Radiation	SW and LW up and down		
VISSS	Precipitation imaging		

Table 3.4.1 Variables measured by the from the 11 m tower and 23 m mast and guest systems maintained by the SEB Flux Team including data recovery rate for December 15, 2019 to February 23, 2020

Figure 3.4.5 23 m mast swaying in high wind event on . This installation was originally 30 m and is registred in sensor web as 30mflux. (Photo Credit: Michael Gallagher)

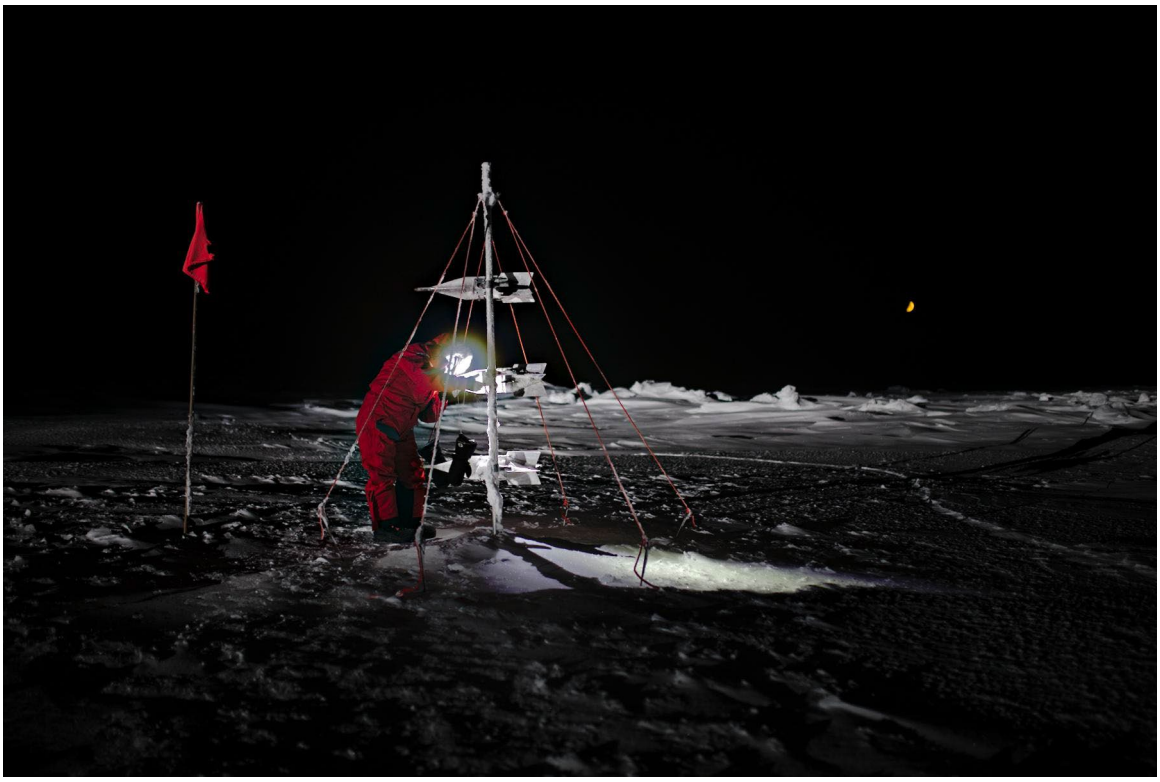

Figure 3.4.6 – Sample collection and positioning of Rocket Traps in Snow 1 (Photo Credit: Michael Gallagher)

Figure 3.4.7 (a) Before cleaning sodar (Photo Credit Michael Gallagher) (b) After Cleaning Sodar (Photo Credit Taneill Uttal)

One of the Met City casualties of the ice movement at the beginning of PS122/2 appeared to be the pycnocline spar and imager buoy systems (T. Stanton, San Jose State University). Several attempts were made to reboot/reconnect the data system as well as examining the integrity of the cabling and connectors between the Met Hut and the buoy heads. This was unfortunately unsuccessful and no data was collected from these systems.

Distributed Network. The distributed network is described in section 1.0 Overview , including a description of the sea-ice and ocean buoys that were co-located with the Autonomous Surface Flux Stations (ASFS) that are discussed in this section (Figure 3.4.8). The ASFSs provide a single level of micrometeorological measurements (T_{air}, P, RH, snow depth, conductive fluxes, T_{sfc}) consistent with the lower 12 m tower level and well as the radiation measurements (SW↓, SW↑, LW↑, LW↓) made at Met City by ARM and FMI; the intent is to determine horizontal variability of the separate components of the SEB balance. Instruments include one sonic anemometer, Vaisala temperature, pressure, and relative humidity measurements, a sonic snow depth sensor, an infrared (surface) thermometer, a GPS system, two cameras, and a set of up- and down-welling longwave and shortwave radiometers. A Licor sensor for measuring

fast water vapor was not operating during Leg II as the heating required to de-ice the sensor required too large of a power draw during the cold winter temperatures.

Figure 3.4.8 ASFS 40 at L1 on December 22, 2019. Note that although the sled structure had snow and ice buildup that the instruments were staying successfully clear of ice and snow through carefully designed heating and ventilation system.

At the end of Leg 1, ASFS-40 at L1 and ASFS-30 at L2 were communicating successfully and reliably by radio. ASFS-50 at L3 which further away was communicating by iridium. The stations that were communicating by radio could be monitored in real time. (Figure 3.4.9). In addition to allowing daily perusal of data for interesting events, the position data provided by the system became an important component of ground support for the helicopter operations both for ALS scan flight plans and visits to the L-sites. For the stations reporting by iridium or only partially by radio, the method for full data recovery is to retrieve data cards during site visits. During PS122-2 a number of remote communication problems occurred. The iridium communications for ASFS-50 at L3 failed on December 12 which was one day before the Dranitsyn arrived at the ice camp with the PS122/2 teams. Several attempts at trouble shooting did not resolve the problem which became low priority as the ASFS-50 at L3 began unexpectedly reporting by radio on an intermittent basis. During PS122/2, the continuity and rate of radio communications for L1 began to deteriorate as the station moved further away from the *Polarstern*. Table 3.4.2 shows the PS122/2 site visits and provides a brief summary of site activities during those visits. For completeness this table also includes all site visits from PS122/1. The primary operational issue that suffered by the ASFS flux stations was continual icing of the exhaust ports resulting in large ice formations; these were removed at each site visit. On Jan 25, the exhaust freeze up at L3 (ASFS-50) appeared to overcome the system resulting in a fuel system failure and shutdown. On Jan 30, the fuel system was restored but a week later on February 6 the system was discovered dramatically capsized by a ridge system (Figure 3.4.10).

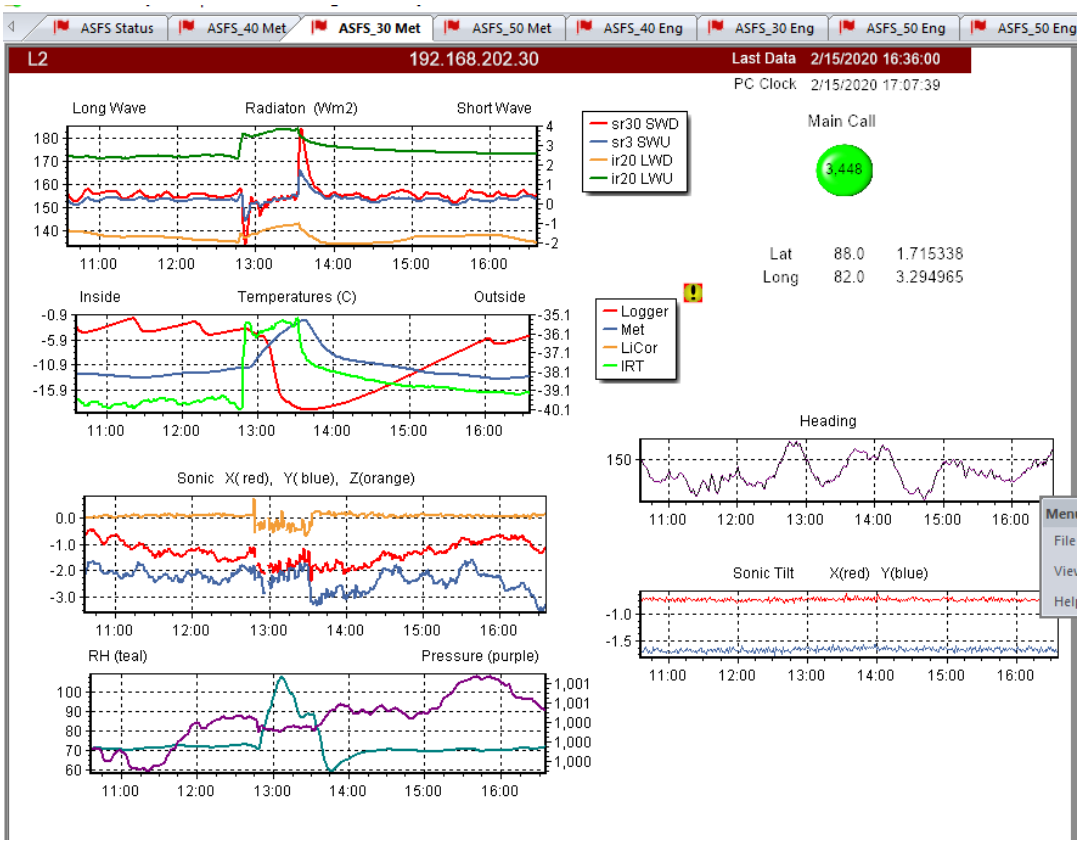

Figure 3.4.9 – Real time displays from ASFS-30 at L2. This figure shows the impact of the helicopter on the sonic wind measurements at 13:00 UTC as well as the effect on internal temperature of opening the system interface box.

With support from the logistics and hell teams, the data card, fueling system and some instruments were retrieved over a two day period (Feb 9-10). The ASFS-50 sled was moved to a safe location and the fuel was removed from the site.

Date	Site	Brief summary of activities
20191005	L1 (ASFS40)	Set up site . Extensive documentation, incl. snow depth.
20191007	L2 (ASFS30)	Set up site. Extensive documentation, incl. snow depth.
20191010	L3 (ASFS50)	Set up site Oct 9-10. Extensive documentation, incl. snow depth.
20191015	L1 (ASFS40)	Re-visit of L1 from Federov, remove Licor from operation
20191016	L2 (ASFS30)	Re-visit of L2 from Federov, remove Licor from operation
20191106	L2 (ASFS30)	Change LWD ventilator. Fuel change. Basic maintenance, incl. snow depth measurements
20191110	L1 (ASFS40)	Swap dead EFOY. Fuel change. Basic maintenance.
20191114	L3 (ASFS50)	Fuel change. Basic maintenance, incl snow depth measurements.
20191114	L2 (ASFS30)	Assess failure. Found bear damage to the station. Retrieved the EFOY and batteries.
20191122	L2 (ASFS30)	Remove damaged equipment from bear damage. EFOY exhaust system, IRT, SWD and a part of the RF antenna cable. Installed replacement sonic anemometer
20191130	L2 (ASFS30)	Re-install full EFOY system including rebuilt exhaust, IRT cable, SWD cable, radio cable, swapped SWU instruments, straightened Met mount, basic maintenance, No fuel swap needed.
20191206	L2 (ASFS30)	Fix the IRT (found blown fuse), measure snow depth, tape sonic box connectors.
20191206	L3 (ASFS50)	Fuel change. Basic maintenance. Assess and change PTU system. Assess SR50 (no issue observed). Turn off power to licor.
20191207	L1 (ASFS40)	Fuel change. Basic maintenance. Taped the sonic box connectors. Some exhaust beard. Snow in SR50. IRT bracket was loose-tightened. Snow depth measurements. No other issues.
20191222	L1 (ASFS40)	First flight to L-site for Gallagher/Uttal and helicopter crew. Landing lights were replaced. There is a new ruggedized battery system being implemented that should facitate lifetime. ASFS40 was visually checked. Soncs ad radiometers are clear. Large exhaust ice sculpture removed - does not seem to be impairing exhaust
20191223	L2 (ASFS30)	Replace Landing Lights
20191223	L3 (ASFS50)	Replace Landing Lights
20191223	L3 (ASFS50)	Second flight of the day to L3 - Visual system check (Gallagher). Cleared exhaust system ice build up.
20191223	L2 (ASFS30)	Second and third flight of the day to L2 - Fuel replacement - Gallagher and logistics bear guard, Haas as methanol minder. Visual inspection and cleared exhaust system ice build up
20191228	L1 (ASFS40)	Replaced SD card. Cleared exhaust ice
20191228	L2 (ASFS30)	Replaced SD card. Cleared exhaust ice

20191228	L3 (ASFS50)	Replaced SD card. Cleared exhaust ice
20200106	L1 (ASFS40)	Refueled. Site Survey by B.Rabe and M. Gallagher.
20200106	L3 (ASFS50)	Refueled. Replaced Sdcard. Site Survey by B. Rabe and M. Gallagher.
20200106	L2 (ASFS30)	Site Survey by B. Rabe and M. Gallagher.
20200108	L3 (ASFS50)	Site Visit to disconnect radio. No site visit folders created since no photos or Sdcard data.
20200111	L1 (ASFS40)	Reset Fuel switch
20200111	L3 (ASFS50)	Upload logger updates (comms issue). Retreived SD card. Snow measurement 15 cm
20200117	L1 (ASFS40)	Team Ice visited and cleaned exhaust and took photos
20200117	L3 (ASFS50)	Team Ice visited and cleaned exhaust and took photos - also noted that there is a narrow crack which is less than a meter about 4-5 meters from L3. The crack is already frozen over and filling with snow.
20200120	L2 (ASFS30)	Refuel and data card swap. Standard Maintenance and Checks.
20200120	L1 (ASFS40)	Data card swap. Standard Maintenance Checks.
20200120	L3 (ASFS50)	Data card swap. Standard Maintenance Checks.
20200122	L2 (ASFS30)	Team ICE journeyed to L2 by Skidoo. Cleaned Exhaust
20200125	L3 (ASFS50)	Welness Check on L3 that had no radio pings and showed a last inside box temperature of -19 degree C. The system was not immediately in danger from near by cracks/leads but was down. Apparently due to complete exhaust freezeup/blockage. Sdcard, Batteries and exhaust system retrieved.
20200130	L3 (ASFS50)	EFOY SWAP for L3. The L3 Batteries were recovered on 1/25/ but there was not a successful warming and recharging. The warming location was the helicopter hanger and both the battaries ruptured while warming. Consequently the spare batteries had to be used: This has creating an issue with connections as the spares (ahem) do not have the same size posts. How it went: MIchael and MIsha (bear guard) flew out and set up camp. The helicopter came back and got Taneil and the toasty EFOY set up. Michael made the swap. We hung around for a couple of hours to see if everything came on and they EFOY kept running. Everything looked good before we left except the sonic. It may have still been warming up. NOTE: Chris got some spare-spare batteries before leaving Tromso
20200202	L1 (ASFS40)	Sdcard retrieval. Blocked section of intake vent - IR camera showed it to be a large heat loss source. Box temperatures have been out of range cold.
20200206	L3 (ASFS50)	**ASFS-50 found tipped up in ridge. Sonic trashed. Boom bent and vaisala intrument looked damaged. Unable to open box to retreive SD card. Unable to fully assess as helicopter called back to ship**
20200209	L3 (ASFS50)	System Secured with anchors to ice. Large Lead has now opened up next to the ridge that ASFS-50 is buried in. SD card retreived. Batteries retreived.

20200210	L3 (ASFS50)	System back on skids. Moved to flat area near surviving buoys - there have also been 2 buoy casualties at L3. Licor and Vaisala instruments recovered. EFOY recovered. Radiometers, SR50, GPS, Radio and IRT look intact. Radio antenna and Interface box appears intact. Frame appears intact. Slid nicely to it's new location.
20200215	L1 (ASFS40)	Sdcard retrieval. Refueled. Likely automatically switched tanks.
20200215	L2 (ASFS30)	Sdcard retrieval. Added foam to intake vent. Refueled.
20200303	L2 (ASFS30)	Trip by Skidoo with Leg 3. EFOY SWAP.

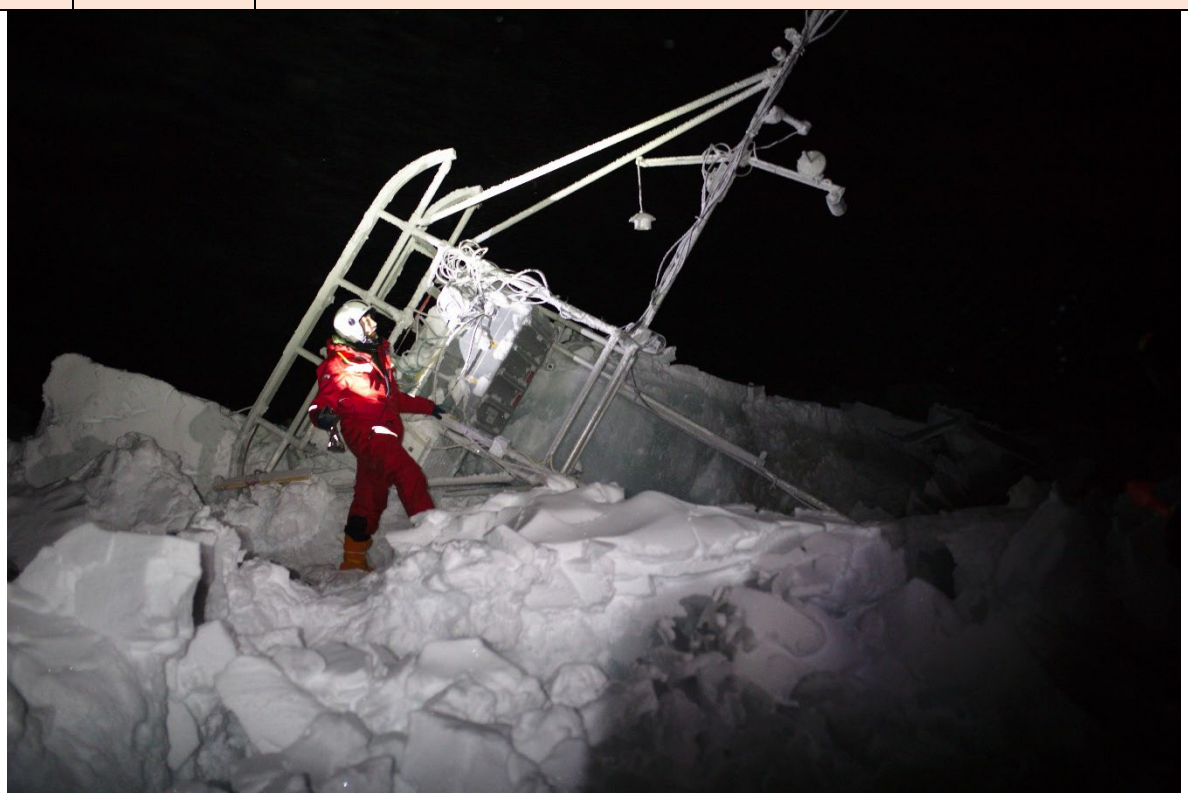

Figure 3.4.10. ASFS-50 at the L3 site discovered inside a ridge system on February 6, 2020

Figure 3.4.11 ASFS-50 after recover and relocation on February 10, 2020

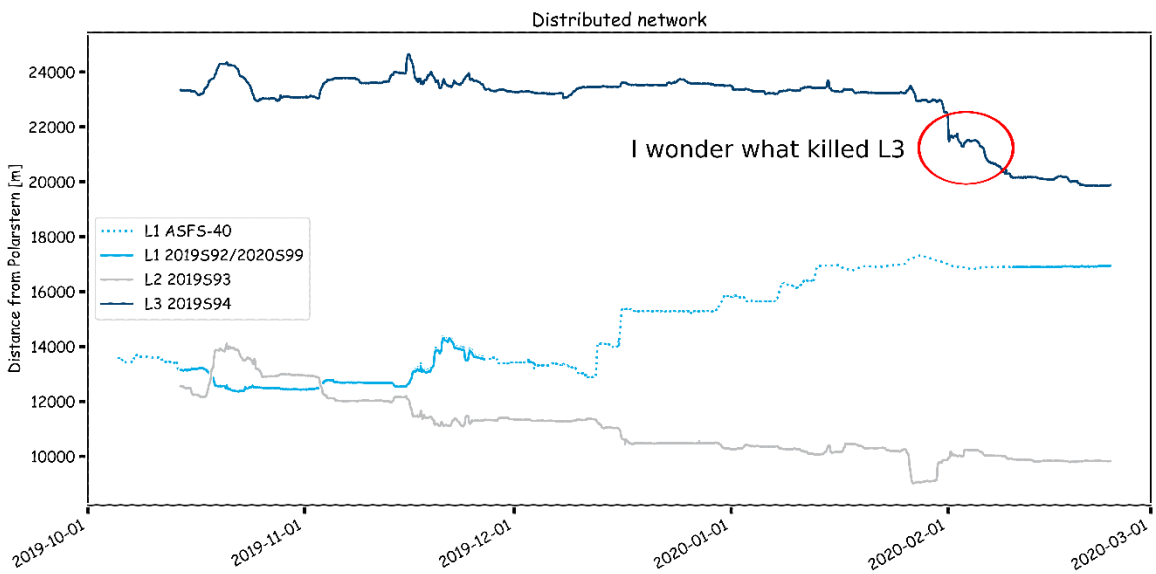

Figure 4.3.12 Distance of L1, L2 and L3 sites from the Polarstern. Locations are from snow buoys (solid lines) and ASFS-40 for L1 after snow buoy was failed and before it was replaced (dotted line). Figure courtesy of A.Jutilla.

Preliminary (expected) results

There are a multitude of temperature on and around the *Polarstern,* with instruments with different sensors at different locations, heights located in air, snow, ice and the ocean. At Met

City alone there are more than 10 different temperature observations. It is expected that for the atmospheric near surface boundary layer that 4 temperature records at 2 m, 6m, 11m from the Met City tower and the 23 m temperature from the mast will be definitive. Fig. 4.3.13 shows these temperatures for the PS122/2 period.

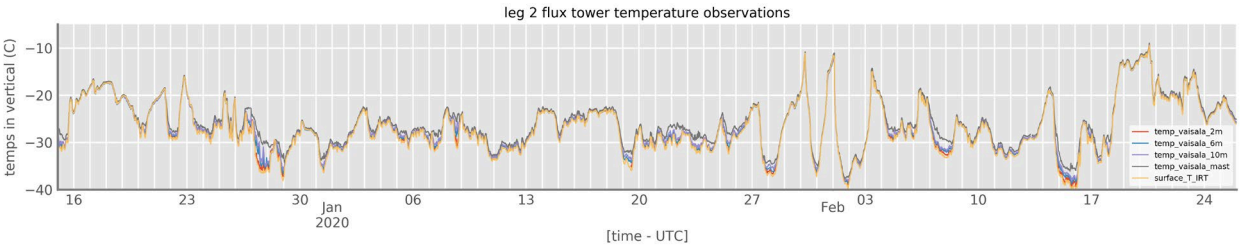

Figure 4.3.13 Temperatures observed at the MOSAiC 'Met City' tower and mast during PS122/2. Also shown is the IRT Surface Temperature.

Because of numerous requests for temperature information during PS122/2, a local website was developed with real time updates on the temperature structure since it often occurred that the DSHIP 29 m measurement of temperature was significantly warmer than the temperature at 2 m which was a more representative working level. Figure 4.3.14 shows a screenshot from the website (http://192.168.6.55:8081/) inset in the DSHIP record showing that on Feb 15 that the surface temperatre was over 5ºC colder than the D-ship value. This website could be further developed to show wind speeds at these levels as well as wind chill.

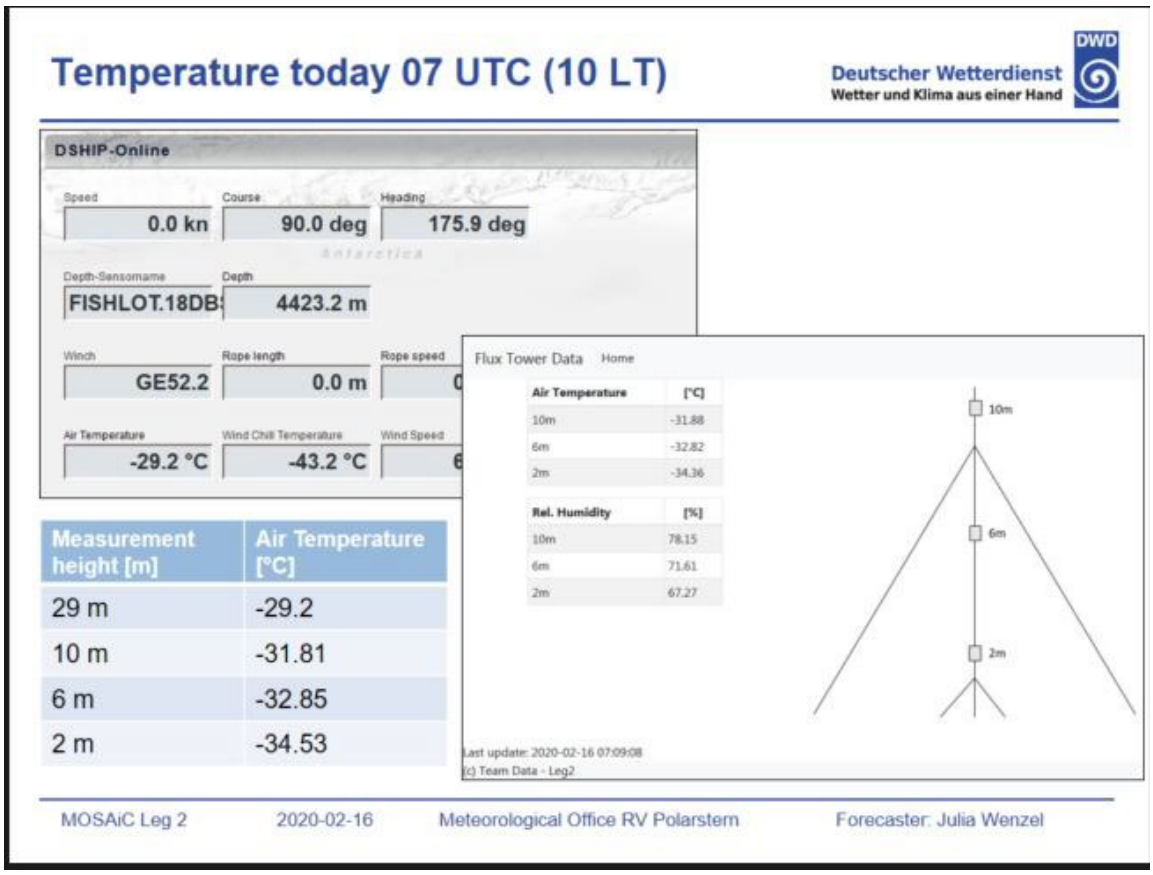

Figure 3.4.14 : Tower temperature measurements from onboard website http://192.168.6.55:8081/ compared to Dship value.

From the time series of temperature observations during leg 2, several features stand out. There are periods of strong temperature inversions as well as several large temperature fluctuations shown in the record. Here we will show results from observations during the more extreme warming events observed on leg 2. There are three events

From the time series of temperature observations during leg 2, several features stand out. There are periods of strong temperature inversions as well as several large temperature fluctuations shown in the record. Here we will show results from observations during the more extreme warming events observed on leg 2.

Figure 4.3.14 shows basic atmospheric parameters impacting the energy budget at the ice sheet surface during late January. On the 28th of January, 2020, atmosphere and snow surface temperatures began at nearly -40C with energy fluxes coming out of the ocean through the sea ice. Onwards, from January 29th and into the 30th, temperatures began to climb with a rapid spike to nearly -10C ocurring at noon UTC on the 30th. The plot shown above also includes important surface energy budget parameters, showing the corresponding variability in long-wave radiation, wind speeds, and turbulent heat fluxes. There is a steep increase in downwelling longwave radiation tied to the increasing temperatures beginning at 12:00 noon on the 28th, likely tied to increasing cloudiness. At the peak temperature on the morning of the 30th, winds reach between 9 and 15 m/s resulting in a negative turbulent heat flux near the surface. Following these peak winds, temperatures sharply decrease after 6:00 UTC and within 12 hours reach significantly below -30C.

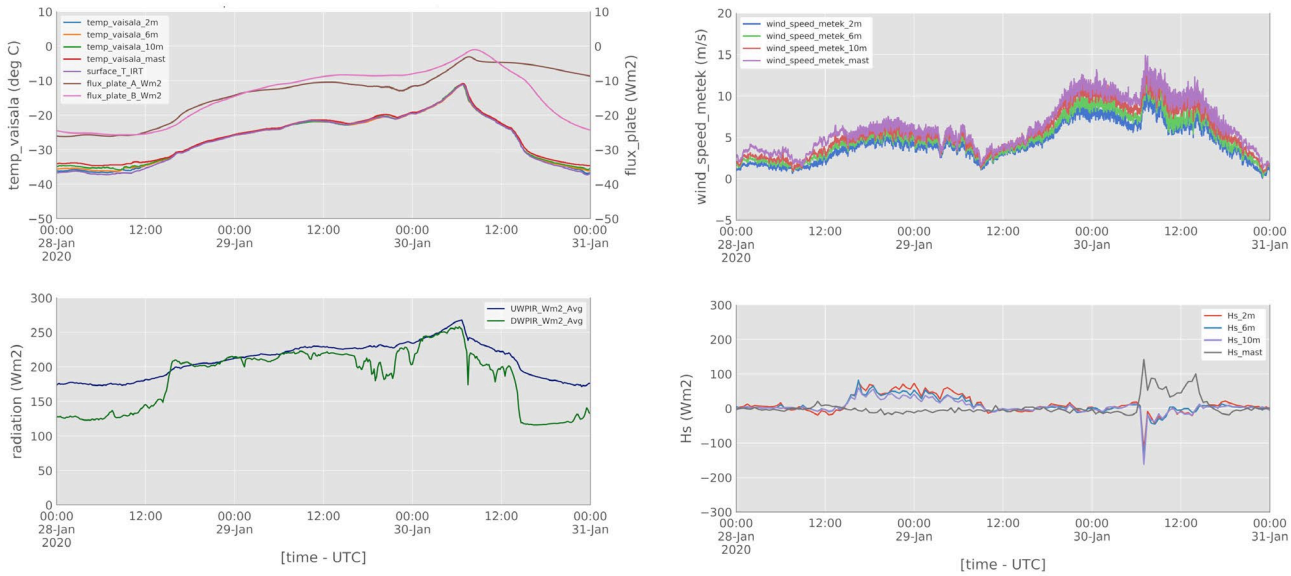

Figure 4.3.15 All observations shown here were made by instruments located in 'Met City' on the MOSAiC ice floe.(top left) The left axis shows temperatures observed in the vertical (2m, 6m, 10m, 23m, and surface) plotted against the right axis showing the energy flux measured by flux plates placed at the snow-ice interface.
(top right) Wind speeds measured by sonic anemometers at the same 4 heights in the vertical
(bottom left) upwelling and downwelling long-wave radiative fluxes observed near ice surface
(bottom right) turbulent heat fluxes derived from sonic anemometer at the same 4 heights

Compared to the event two days previous, the temperature increases leading to the maximum on February 1st at midnight are less steep (Figure 4.3.16). One notable difference of this particular event is the temperature plateau on the evening of January 31st , with evening temperatures remaining above -15C for nearly 12 hours. During this plateau, the energy flux through the sea ice remains very near to zero. At approximately 02:00 on the 31st temperatures drop sharply, decreaseing 20C in less than 4 hours as wind speeds increase from 0 to nearly 20 m/s as observed on the 23 meter mast. There is also increased downwelling

long-wave radiation on the morning of the 31st, likely tied to increased cloud cover, lasting until the steep temperature decrease. Alongside the rapid wind speed increase and steep temperature drop, there is a related negative turbulent heat flux.

On February 18th (Figure 4.3.17), after temperatures rose to above -15C, the energy flux out of the sea ice remained near-zero for the duration of more than three days. This flux was driven by significant increases in downwelling long-wave radiation, as well positive turbulent heat fluxes at the surface.

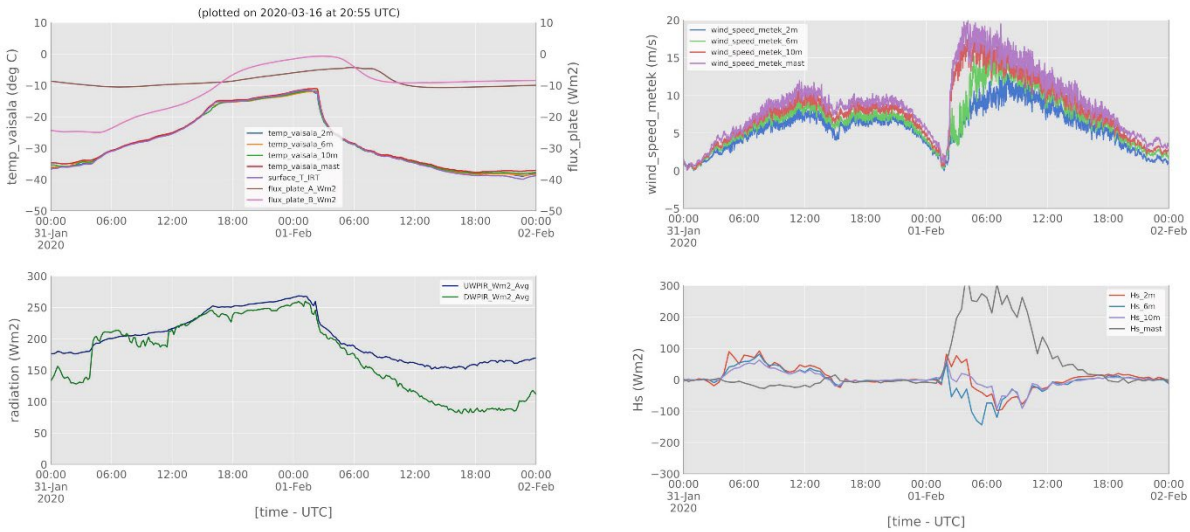

Figure 4.3.16 Observations made by instruments located in 'Met City' on the MOSAiC ice floe, presented in the manner of previous Figure.

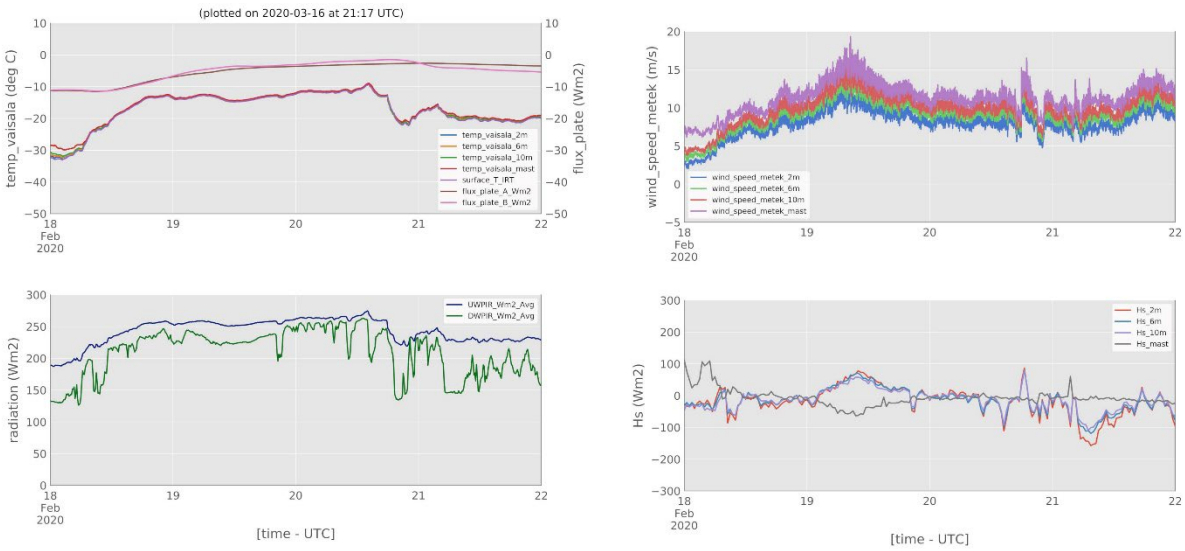

Figure 4.3.15 Observations made by instruments located in 'Met City' on the MOSAiC ice floe, presented in the manner of previous Figure.

Data management

The data described in this section were continuous and were not associated with any event logging. The data collected by the many instruments on the 11-m tower in combination with the the 23 m (formally 30 m) mast and the CLASP uploaded to the MCS under the sensor web

platform “flux_tower_12m_ucb”. Data for the 3 flux stations were uploaded to the MCS under the sensor web platforms asfs_30_ucb, asfs_40_ucb and asfs_50_ucb.

References

No references

3.5. TRACE GAS FLUX GROUP

Dean Howard[1,2]

(not on board:) Byron Blomquist[1,2], Detlev Helmig[1], Steve Archer[3], Laurens Ganzeveld[4], Jacques Hueber[1], Christopher Fairall[2], Dean Howard[1], Ludovich Bariteau[1,2], Kevin Posman[3], Hans-Werner Jacobi[5], Helene Angot[1], Sjoerd Barten[4], William Sturges[6], Lucy Carpenter[7]

[1]EDU.CU
[2]GOV.NOAA
[3]ORG.BIGELOW
[4]NL.WUR
[5]FR.UGA
[6]UK.AC.UEA
[7]UK.AC.YORK

Objectives

Continuation of the three measurement campaigns commenced during Leg 1 (Blomquist et al., 2020). Namely, these three measurement series were 1. continuous eddy covariance of the four primary gas species of interest -- carbon dioxide (CO2), methane (CH4), dimethyl sulfide (DMS) and ozone (O3), 2. continuous mean and flask measurements of volatile organic compounds (VOCs), halogenated compounds, nitrogen oxides (NO/NO2) and gaseous elemental mercury (GEM), and 3. dynamic flux chamber measurements of the four primary gases, in conjunction with measurements from other Leg 2 MOSAiC teams.

In addition to those measurement systems installed during Leg 1, a NOx/NOy conditional sampling inlet was installed in conjunction with the NO/NO2 chemoluminescent system, and flask sampling for halogenated gas species was brought in alongside the NOAA GMD carbon compound sample flasks. Additional testing and development of the O3 dynamic flux chamber system was also completed, as well as the installment of a gradient-based micrometeorological flux system for O3 on the Met City 12 m tower and all instrumentation necessary for an O3 snow-air gradient tower. The physical installation of this latter tower was unable to be completed due to limited available manpower and will be installed during the Leg 3 campaign.

Work at Sea

Table 3.5.1 below shows an updated list (from Table 3.6.1, Blomquist et al., 2020) of all measurement systems currently deployed within the MOSAiC trace gas flux group for Leg 2. Note that the DMS API Mass Spectrometer is not listed here, as it suffered a loss of a DC power supply in Leg 1 and will not be operational until Leg 4. Details for these measurement systems can be found in Blomquist et al. (2020).

Tab. 3.6.1: Measurement Systems Deployed for Leg 2

Measurement System	Sampling Location	Sample Rate	SensorWeb ‘Short Name’
DMS API Mass Spectrometer	ship bow tower	10 Hz continuous	dms_apims_ship_bow

Measurement System	Sampling Location	Sample Rate	SensorWeb 'Short Name'
Picarro G2311-f CRDS	ship bow tower	10 Hz continuous	crds_ghg_ship_bow
Chemiluminescent Ozone	ship bow tower	10 Hz continuous	ozone_fast_ship_bow
Metek uSonic-3 Anemometer	ship bow tower	10 Hz continuous	sonic_anemometer_3D_ship_bow
Licor 7500DS	ship bow tower	10 Hz continuous	licor_7500ds_ship_bow
RM Young 86004 Sonic Anemometer	ship bow tower	1 Hz continuous	sonic_anemometer_2D_ship_bow
Chemiluminescent NO/NO2	ship bow crane	10 per minute	nox_ship_bow
TEI model 49C ozone analyzer	ship bow crane	1 per minute	ozone_slow_ship_bow
Tekran 2537B mercury analyzer	ship bow crane	1 per 5-15 minute	hg_ship_bow
Agilent GC Mass Spectrometer	ship bow crane	~15-18 per day	gcms_ship_bow
Picarro G2311-f CRDS	met city 10m tower	10 Hz continuous	crds_ghg_ice_station_tower
CO2/CH4 Flux Chamber	various	1-2 per deployment	co2_ch4_chamber_portable
Ozone Flux Chamber	various	1-2 per deployment	ozone_chamber_portable
Michell S8000 hygrometer	ship bow tower	~1 per minute	t_rh_ship_bow

NOx/NOy inlet
An inlet system designed for measuring NOy species was installed at the sample inlet of the NO/NO2 chemiluminescent instrument. This inlet system is synced in time to the sampling sequence of the NO/NO2 chemiluminescence instrumment, and allows for intermittent quantification of NOy via chemical conversion of NOy species to NO. Switching between dual flow paths (one with chemical conversion of NOy to NO, the other without), gives measurements of NOx as well as NOy as outputs from the NO/NO2 chemiluminescence instrument.
Initial operation of the NOy inlet began on ???. Additional testing of flows and flow paths, as well as calibration procedures, followed. Continuous measurements began on ???.

O3 dynamic flux chamber
Additional development and testing of the O3 dynamic flux chamber took place during Leg 2, building on that commenced during Leg 1. Some repairs to the electrical circuitry were required at first, followed by development of ozonesonde and chamber system conditioning

standard operating procedures. Verification of the accuracy and precision of the sondes was able to be completed once the gradient-based micrometeorological flux system was installed at Met City, by using the differential-mode TEI model 49C ozone analyser. Finally, field sampling procedures were tested and modified so as to eliminate the influence of entrainment of ambient air into the chamber on system blank O3 fluxes. Only one O3 flux measurement deemed reliable (i.e. both field measurement and system blank measurement were acceptable) was taken during Leg 2. However, the O3 dynamic flux chamber system and the operating protocols are now deemed reliable and continued measurements can take place during Leg 3 and beyond.

UEA flask samples
In addition to the NOAA GMD flask samples, flask sampling for halogenated compounds using the University of East Anglia (UEA) flask system began on ???. These also take place according to the weekly NOAA GMD schedule and will be sent to UEA at the end of the MOSAiC campaign for analysis.

CO2/CH4 dynamic flux chambers
Flux sampling of CO2 and CH4 continued during Leg 2, with three regular samples per week scheduled. These took place 1. close to the Met City flux tower for comparison with the eddy covariance CO2/CH4 flux measurements, 2. close to the snow/ice thickness South Transect for comparison with thickness measurements undertaken by MOSAiC Team ICE, and 3. in conjunction with coring sampling undertaken by the MOSAiC Team BGC. Additionally, a lead event that took place on ??? resulted in some additional sampling. Table ??? gives times and locations of all CO2/CH4 chamber measurements during Leg 2.

Preliminary (expected) results
The 2D sonic anemometer/backflush system described in Blomquist et al. (2020) continued to operate well, excluding sampling from sectors that were defined as influenced by the ship's exhaust. Figure ??? below shows the number of hours per day defined as coming from the so-called 'clean sector'. ???How many hours of good data??? It was noted that the NO/NO2 chemiluminescence instrument measured concentration spikes during wind conditions that were margnially within the clean sector (i.e. close to +/- 130 degrees from bow), suggesting an area source of nitrogen compounds from the ship. Additional filtering of NOx/NOy data will hence be required during post-processing.

The Met City CO2/CH4 flux system operated well during Leg 2, with only minimal loss of data due to power failures at the site. ???How many hours of good data???

Actual flux values from the CO2/CH4 dynamic flux chamber system were not yet able to be calculated, due to the unavailability of programming libraries necessary for the scripted code. However, concentration data suggest that fluxes of both species were low and positive (up from the surface). Sampling in conjunction with MOSAiC Team BGC at a lead site suggested slight methane emission that decreased over time. Ice core concentrations and isotopic fractionations additionally point to methane emission to the atmosphere at this site. Not all refrozen leads sampled showed this behaviour of methane emission.

Data management
All data are handled, documented, archived and published following the MOSAiC data policy (see APPENDIX). Raw data from all these systems has been archived in MOSAIC Central Storage (MCS).

3.6. MEASUREMENT-BASED UNDERSTANDING OF THE AEROSOL BUDGET IN THE ARCTIC AND ITS CLIMATE EFFECTS - MBRACE

Ivo Beck[1]

[1]CH.EPFL
[2]FI.UNI-Helsinki

(not on board:) Lauriane Quéléver[2], Julia Schmale[1], Mikko Sipilä[2], Tiia Laurila[2], Tuija Jokinen[2], Zoe Brasseur[2]

Objektives

Low-level clouds have an important effect on the surface energy budget in the Arctic. Their lifecycles and warming and cooling effects over the central Arctic Ocean remain unclear, and models fail to correctly simulate them. This shortcoming is partly due to insufficient information on cloud phase (liquid and/or ice crystals). Particularly liquid droplets modulate cloud radiative properties responsible for warming. Droplets form on cloud condensation nuclei (CCN), a subset of aerosol particles. Aerosol particle concentrations over the central Arctic Ocean can be extremely low such that cloud properties are strongly influenced by CCN availability, and in extreme cases cloud formation is even inhibited. Information on aerosol is scarce for all seasons in the high Arctic, but in particular for the cold and dark period when clouds have a pronounced warming effect. To date, only information from land-based stations further south provide proxy information on central Arctic Ocean aerosols in winter.

We run a laboratory container with state-of-the-art aerosol instrumentation, including high-resolution mass spectrometers, to study new particle formation (NPF, see project on "Formation of secondary nano-sized aerosol particles from atmospheric trace gases and ions in the polar marine environment" by T. Jokinen et al.), particle growth, the chemical composition of the particles, and activation of particles to cloud droplets. We operate the instrumentation behind a total inlet that captures particles and droplets, and an interstitial inlet which captures only particles that are unable to form cloud droplets.

Our guiding research questions are as follows:

- What are the contributions of natural versus anthropogenic sources to central Arctic Ocean CCN concentrations and how do they vary throughout the seasons (e.g. full sea ice cover in winter vs marginal ice zone in summer)?
- How important is growth of newly formed particles for the CCN budget?
- Which key natural processes are likely to change the CCN budget and control cloud properties with global warming (e.g., diminishing sea ice)?
- How strongly are liquid cloud radiative properties controlled by availability of CCN throughout the seasons?
- What are natural sources of aerosol in general and CCN in particular during polar night?

With our dataset, we will shed light on the contribution of anthropogenic emissions that are not greenhouse gases to Arctic warming through cloud formation, characterize for the first time aerosol-cloud interactions during Arctic winter, and help to evaluate and improve models for better predictions of Arctic climate change and its far-reaching consequences.

Work at sea

Real-time measurements are carried out in the Swiss aerosol container (starboard/bow, position C10 on Polarstern) and the British Antarctic Survey container (adjacent) by one person during all legs. The main tasks of the operator include: Guarantee high quality

performance of the complex instrumentation, capturing natural and anthropogenic events that influence aerosol characteristics, and taking (or have taken) snow samples after fresh snowfall for subsequent on-shore laboratory analyses.

Expected results

We collected a continuous dataset of Leg 2 (December 9th until February 26th) for almost all our instruments (see Table 1 below for specific instruments measurement periods). Our dataset includes data of very clean atmospheric conditions as well as data of contaminated air. Contamination was mainly caused by the ship's exhaust, sometimes also by the Pistenbully's activities. According to the ship's visibility data we only experienced smaller fog events on December 19 and December 20 (Figure1). In January and February we recorded the start of the arctic haze (Figure 2), showed in an increasing background Aerosol number concentration during clean conditions.

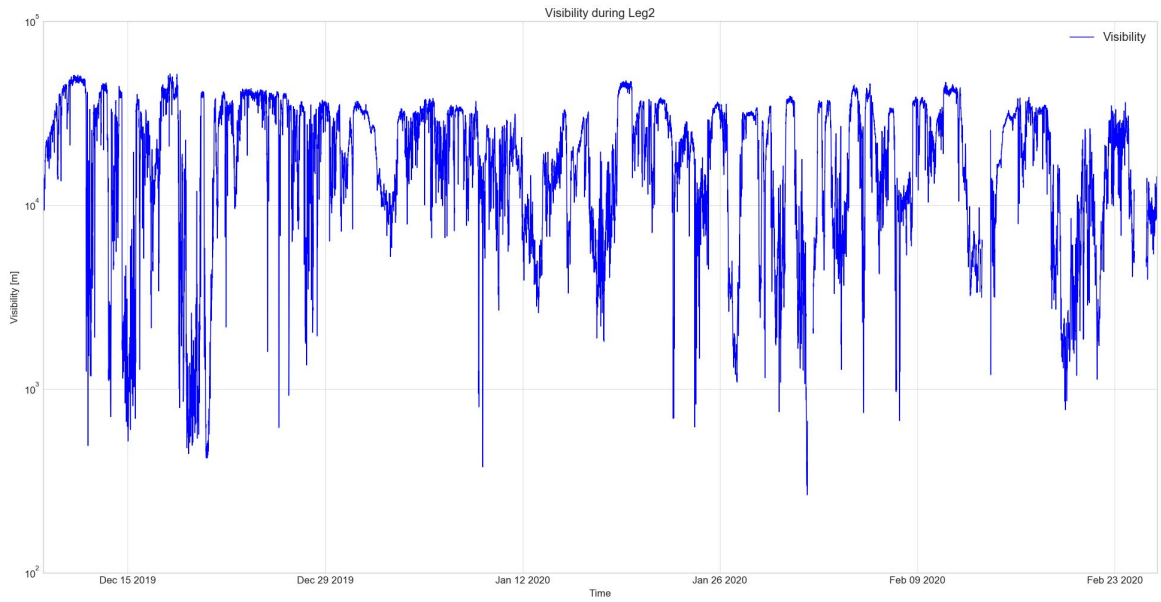

Figure 1: Visibility during Leg 2

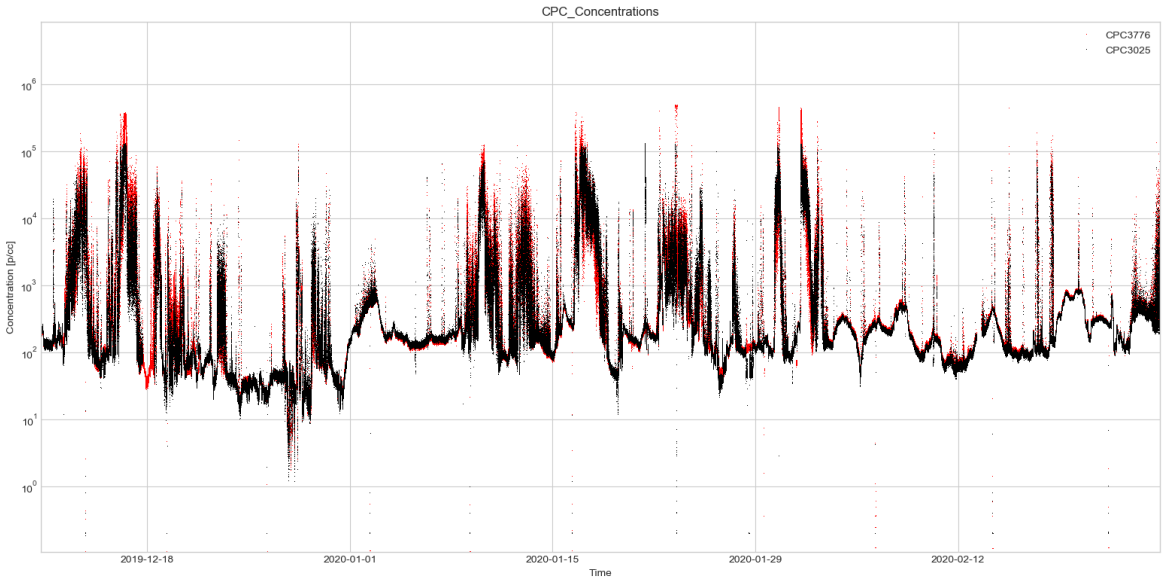

Figure 2: CPC raw data of interstitial (black) and total (red) inlet

Instrument performance

With a few exceptions, all instruments have been sampling during the whole period. An overview of all instruments and their working periods is shown in Table 1. Smaller data gaps usually lasted less than one day and are not listed.

Id	Instrument	Location - Inlet	Application	Samplig period
CPC 3776	Condensation particle counter	C10 – Total	Aerosol concentration of the total particle population	09.12.2019 – 26.02.2020
CPC 3025	Condensation particle counter	C10 - Interstitial	Aerosol concentration of the ultrafine particle population (i.e. diameter < 1 µm)	09.12.2019 – 26.02.2020
CPC 3010	Condensation particle counter	C10 – Interstitial & Total	Aerosol concentration of the size selected particle. Used for scanning mobility particle sizer measurement and aerosol mass spectrometer calibration	09.12.2019 – 26.02.2020
PSM A11-1 & A11-2	Particle size magnifier	C10 - NPF	Size distribution of the smallest aerosol particles from 1.5 to 3 nm Two identical instruments are run in parallel for scanning and stepping mode inter-comparison	09.12.2019 – 26.02.2020
CPC A11-1 & A11-2	Condensation particle counter	C10 - NPF	Used for detection of particle size magnifier setups A11-1 & A11-2	09.12.2029 – 26.02.2020
NAIS	Neutral cluster and air ion spectrometer	C10 – NPF	Size distribution of both neutral and naturally charged cluster population for electrical mobility equivalent diameter ranging from 2 to 40 nm	09.12.2019 – 13.02.2020 15.02.2020 – 26.02.2020
SMPS	Scanning mobility particle sizer	C10 – Interstitial & Total	Size distribution of the aerosol population for electrical mobility equivalent diameter ranging from 10 to 1000 nm	09.12.2019 – 26.02.2020
APS	Aerodynamic particle spectrometer	C10 - Total	Size distribution of the large aerosol population for aerodynamic equivalent diameter ranging from 0.5 to 20 µm	09.12.2029 – 26.02.2020
CCNC	Cloud condensation nuclei counter	C10 – Interstitial & Total	Aerosol concentration for potential growth cloud condensation nuclei at several supersaturation ratio on hourly cycle	09.12.2019 – 26.02.2020
Wibs	Wibs	C10 - Total	Measurement of fluorescently active aerosol for biological speciation	09.12.2019 – 26.02.2020
Aethalometer	Aethalometer	C10 – Interstitial & Total	Measurement of black carbon	09.12.2019 – 26.02.2020
AMS	Aerosol mass spectrometer	C10 – Interstitial & Total	Chemical compotion of aerosol particle (e.g. sulfate, nitrate, organic, ammonium, chloride, …)	Did not work during the whole period due to a failure in the electronics.
CI-APi-TOF	Nitrate-based chemical ionization atmospheric pressure interface time of flight mass spectrometer	C10 - NPF	Measurement of the chemical composition of gas-phase compound and highly oxidized molecules, precursors of aerosols (e.g. Sulfuric acid, iodic acid, …)	09.12.2019 – 26.02.2020
APi-TOF	atmospheric pressure interface time of flight mass spectrometer	C9 - roof	Measurement of the chemical composition of gas-phase naturally charged ions, precursors of aerosols (e.g. Sulfuric acid, ammonia clusters, …)	09.12.2019 – 14.02.2020, 17.02.2020 – 26.02.2020
O3	Ozone monitor	C10 - Interstitial	Ozone concentration	09.12.2019 – 22.01.2020; 01.02.2020 – 26.02.2020
SO2	SO2 monitor	C10 - Interstitial	Sulfur dioxide concentration	09.12.2019 – 26.02.2020

Picarro	Picarro Analyzer	C10 - Interstitial	Gas-phase concentration of Methane, Carbon monoxide, Carbon dioxide, water vapor	09.12.2019 – 26.02.2020
RH / T 1 & 2	Hygrometer	C10 – Interstitial & Total	Relative Humidity and temperature sensor for both Interstitial and Total inlet	09.12.2019 – 26.02.2020
V1	Valve switch	C10 – Interstitial & Total	Hourly bases inlet sample switch for AMS, CCNC, Aethalometer, SMPS	09.12.2019 – 06.02.2020
HiVol*	High volume filter sampler	C9 - roof	High volume aerosol filter (Borosilicate, pore ⌀ 1.6 µm 800 Lpm) sampling weekly	09.12.2019 – 26.02.2020
LoVol*	Low volume filter sampler	C9 – roof	High volume aerosol filter (Polycarbonate, pore ⌀ 0.2 µm // 20-25 Lpm) automated 48 h cycle sampling	09.12.2019 – 26.02.2020
Grimm OPC*	Optical particle counter	C9 – roof	Aerosol concentration of big particles	09.12.2019 – 05.02.2020
Filter Tropos**	Filter sampling	C9 – roof	Aerosol filter (Polycarbonate, pore ⌀ 0.8 µm) sampling weekly	09.12.2019 – 10.01.2020

Table 1: All instruments and their Sampling Periods during Leg 2